Proc. R. Soc. Lond. B **231**, 251–288 (1987)
Printed in Great Britain

Spatial properties of neurons in the monkey striate cortex

BY M. J. HAWKEN AND A. J. PARKER
University Laboratory of Physiology, Parks Road, Oxford OX1 3PT, U.K.

(*Communicated by H. B. Barlow, F.R.S. – Received* 21 *November* 1986)

Contrast sensitivity as a function of spatial frequency was determined for 138 neurons in the foveal region of primate striate cortex. The accuracy of three models in describing these functions was assessed by the method of least squares. Models based on difference-of-Gaussians (DOG) functions were shown to be superior to those based on the Gabor function or the second differential of a Gaussian. In the most general case of the DOG models, each subregion of a simple cell's receptive field was constructed from a single DOG function.

All the models are compatible with the classical observation that the receptive fields of simple cells are made up of spatially discrete 'on' and 'off' regions. Although the DOG-based models have more free parameters, they can account better for the variety of shapes of spatial contrast sensitivity functions observed in cortical cells and, unlike other models, they provide a detailed description of the organization of subregions of the receptive field that is consistent with the physiological constraints imposed by earlier stages in the visual pathway. Despite the fact that the DOG-based models have spatially discrete components, the resulting amplitude spectra in the frequency domain describe complex cells just as well as simple cells. The superiority of the DOG-based models as a primary spatial filter is discussed in relation to popular models of visual processing that use the Gabor function or the second differential of a Gaussian.

INTRODUCTION

A major contribution to our understanding of early visual processing, mainly originating from psychophysical studies in humans, is that the initial stages of the spatial analysis of a visual scene can be considered as a consequence of the operation of a set of spatial bandpass filters on the retinal image (Campbell & Robson 1968; for review, see Braddick *et al.* 1978). A number of models of detection and discrimination judgements in human visual perception have incorporated spatial bandpass filters as crucial components (Wilson & Bergen 1979; Watson 1983; Watt & Morgan 1985). The implementation of procedures for image processing (Marr & Hildreth 1980; Yuille & Poggio 1985) is often based on bandpass mechanisms similar to those proposed in psychophysical models. It is generally thought that the neural mechanisms underlying such a set of bandpass filters are provided by cells in the primary visual cortex (Cooper & Robson 1968; Blakemore & Campbell 1969; Robson 1975; Marr & Hildreth 1980; Sakitt & Barlow 1982; Robson 1983; Watson 1983).

Hubel & Wiesel (1962, 1968) discovered that the majority of neurons in the primary visual cortex of cat and monkey are selectively sensitive to the orientation of edge or bar stimuli and they categorized them into two main classes: 'simple' and 'complex'. Characteristically, simple cells show discrete subregions in their receptive fields (Hubel & Wiesel 1962) and linear spatial summation (Movshon *et al.* 1978*a*). Complex cells, on the other hand, do not have spatially separated 'on' and 'off' regions in their receptive fields (Hubel & Wiesel 1962) and show nonlinear spatial summation (Movshon *et al.* 1978*b*). Both classes generally exhibit bandpass characteristics as a function of spatial frequency in their responses to drifting gratings and their sensitivity to the contrast of such patterns (Movshon *et al.* 1978*a*, *b*; DeValois *et al.* 1982) but the linear properties of simple cells would seem to make them better candidates for the spatial filtering of the image (Robson 1975; Marr 1982).

The primary visual cortex receives its principal afferent input from the dorsal lateral geniculate nucleus (LGN), the cells of which have roughly concentrically arranged receptive fields with spatial antagonism between the centre and the surround (Hubel & Wiesel 1961; Wiesel & Hubel 1966). Hubel & Wiesel (1962) proposed that a cortical simple cell with an even-symmetric receptive field could be made up of inputs from a row of geniculate-cell receptive fields flanked by rows of inputs from geniculate-cell receptive fields of the opposite sign. It seems reasonable to suppose that cortical cells showing linear spatial summation are primarily influenced by neurons also showing linear summation. The major classes of geniculate relay neurons in the primate with this property are linearly summating 'X-cells' in the parvocellular and magnocellular layers of the LGN (Blakemore & Vital-Durand 1981; Shapley *et al.* 1981; Derrington & Lennie 1984).

In this paper we attempt to find a suitable model for describing the spatial properties of the receptive fields of neurons in the primary visual cortex. A satisfactory model should allow an accurate estimate of the bandwidth, peak spatial frequency, cutoff spatial frequency and peak sensitivity of the neuron's spatial-contrast sensitivity function, as well as reflecting the structural organization of the receptive field as conventionally plotted. We needed such an accurate model of cortical receptive fields to allow us to compare the contrast thresholds of single neurons with those determined psychophysically for human observers (Parker & Hawken 1987). Initially, we chose the Gabor function to provide a smooth fit to the spatial-contrast sensitivity functions of cortical neurons because it had been used successfully to describe the spatial-frequency tuning functions of neurons in the cat's visual cortex (Marčelja 1980; Kulikowski & Bishop 1981; Kulikowski *et al.* 1982) and was also the basis for some models of visual processing (Sakitt & Barlow 1982; Watson 1983; Daugman 1984). However, the Gabor model produced generally inaccurate estimates of the shape of the sensitivity function; most notably, the height and location of the peak of the fitted function usually differ from those of the data. We also tried functions based around the second differential of a Gaussian, which have been used extensively in computer vision programs that find edges in images (Marr & Hildreth 1980). The imperfections of these two models led us to the quantitative formulation of a different model, based on the likely organization of the physiological inputs to the visual cortex, which

was qualitatively outlined by Hubel & Wiesel (1962). Here we show that this scheme, which is physiologically plausible but requires many parameters, gives much better fits to the spatial-contrast sensitivity functions than mathematically simpler functions, derived from computational analyses of visual processing, such as the Gabor function or second differential of a Gaussian. In the next section, we describe the new model, as well as the others, in detail.

Models

For simple cells, which show linear spatial summation, the spatial-contrast sensitivity function will be the amplitude portion of a Fourier representation of the receptive-field profile. The shapes of the spatial-frequency tuning function and the spatial weighting function are thus directly related (Movshon *et al.* 1978*a*; Andrews & Pollen 1979; Dean & Tolhurst 1983), although phase information is required for a complete representation (see, for example, Enroth-Cugell *et al.* 1983). In fact any well-specified model of the receptive-field profile must make some prediction of the characteristic shape of the spatial-contrast sensitivity function. Even for nonlinear complex cells, at least in the cat, the inverse transform of the spatial-frequency tuning function relates quite accurately to the 'subunit' structure of the overall receptive field determined by measurements of local summation within the field (Movshon *et al.* 1978*b*) and may provide an accurate measure of the spatial filtering of the receptive field, even though the output is highly nonlinear.

In 1966 Enroth-Cugell & Robson showed that the spatial-contrast sensitivity function of X-cells in the cat's retina could be well described by the difference of two Gaussian weighting functions, a model that was proposed initially by Rodieck (1965). This approach, relating the space and spatial-frequency domains, has been widely used in quantitative analyses of visual processing. The difference-of-Gaussians function, as usually applied to retinal ganglion cells and lateral geniculate neurones, is a rotationally symmetrical function with a single spatial variable, the distance r from the receptive field centre, although deviations from rotational symmetry have been noted (Levick & Thibos 1980; Dawis *et al.* 1984; Soodak 1986).

Many cortical neurons have receptive fields that are elongated in the central excitatory region (correlating with their selectivity for orientation), thus forfeiting the condition of rotational symmetry. But in the direction orthogonal to the elongated axis or preferred orientation, the receptive fields of simple cells have spatially segregated subregions of opposite sign. This is the substructure giving them their bandpass characteristics in spatial frequency. The individual subunits of complex cells may have similar properties (Movshon *et al.* 1978*b*; Spitzer & Hochstein 1985*a*, *b*). Therefore, by constraining the comparison of cells and models to the dimension orthogonal to the preferred orientation, the bandpass nature of the cell's receptive field can be investigated.

Figure 1 illustrates the general form of some hypothetical spatial weighting functions, in the direction orthogonal to the preferred orientation, of receptive fields with even symmetry (figure 1*b*), intermediate symmetry (figure 1*c*) and odd

symmetry (figure 1*d*). These all have the same bandpass spatial-contrast sensitivity functions (figure 1*a*) in the frequency domain. All realistic models must allow the receptive fields of cells to attain the general shapes of either pure even-symmetric, pure odd-symmetric or somewhere between the two, as shown in figure 1 (Kulikowski & Bishop 1981). The rest of this section is devoted to describing, in detail, the models that are evaluated in this paper.

Models based on difference of Gaussians (DOG) functions

The first model treats each subregion of a simple cell's receptive field as if it were derived from a single lateral geniculate neuron with a difference-of-Gaussians (DOG) profile for its receptive field (Rodieck 1965; Enroth-Cugell & Robson 1966; Derrington & Lennie 1984). Consider, for example, a hypothetical simple cell receptive field with a discrete central 'on' subregion and two flanking 'off' subregions, equally spaced either side of the central region. Such a conventional 'hand-plotted' receptive field is shown in figure 2*a*.

The underlying sensitivity profile of the 'on' region in the hand-plot is itself a DOG (the weighting function of an on-centre LGN cell giving excitatory input to

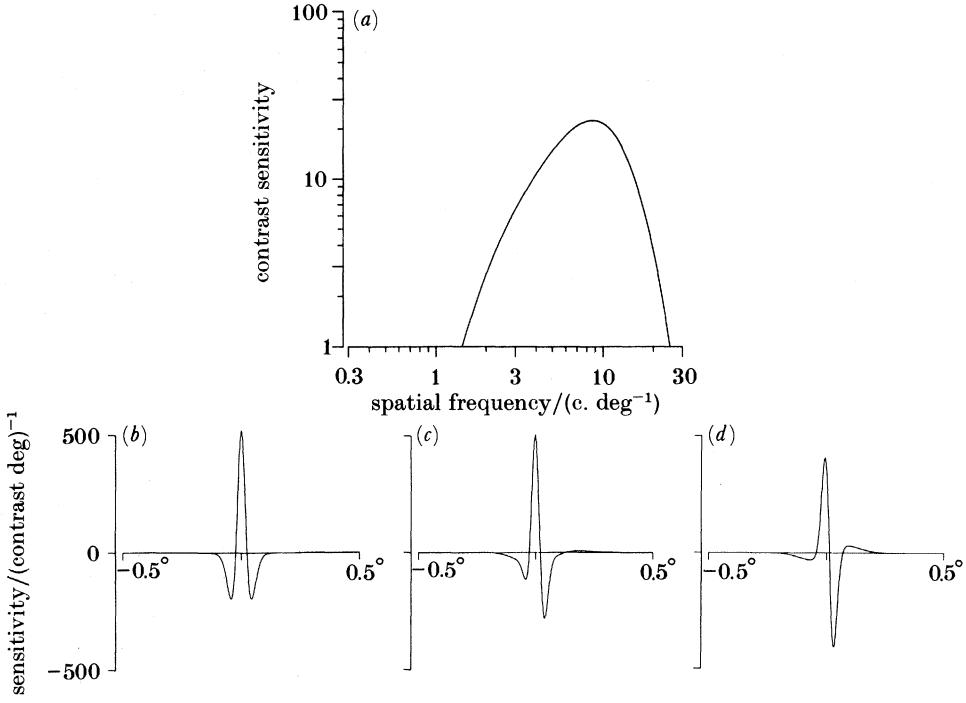

FIGURE 1. The upper graph (*a*) shows a bandpass function, relating contrast sensitivity and spatial frequency, which is typical of the spatial-contrast sensitivity functions found for most neurons in the striate cortex. The lower graphs show three possible inverse Fourier transforms of the amplitude spectrum in the upper graph, indicating the variations of receptive-field organization consistent with this amplitude spectrum when no phase information is available: purely even symmetry (*b*), intermediate (*c*) and purely odd symmetry (*d*).

this simple cell), whose centre component responds to an increment in brightness and whose surround component is of opposite sign. The flanking 'off' subregions of the hand-plot are also each a DOG, but of opposite configuration to that comprising the 'on' subregion (e.g. the weighting functions of off-centre LGN cells). The peaks of the Gaussians forming the flanking 'off' subregions are spatially separated from ones forming the central 'on' subregion. The second row in figure 2*a* gives the spatial profile of each of the separate Gaussians, which make up the receptive field shown in the third row of figure 2*a*. An alternative form of this model may have just two subregions, corresponding to an odd-symmetric receptive field, as illustrated in figure 2*b*. A receptive-field intermediate between pure even and pure odd symmetry, with unbalanced flanking regions, can also be created with this model, by varying the relative amplitudes of the flanking DOGs.

Each component Gaussian in this model must be specified by three parameters: the peak amplitude, spatial location of the peak amplitude and the space constant of the Gaussian. It is mathematically convenient to place the origin of the spatial coordinate system at the location of the peak of the central subregion. This subregion can therefore be specified by four parameters: the space constants of the Gaussians (x_{c_1} and x_{s_1}) and their amplitudes (k_{c_1} and k_{s_1}). In general, a flanking subregion must be specified by five parameters, four of which are equivalent to those describing the centre subregion ($x_{c_2}, x_{s_2}, k_{c_2}, k_{s_2}$) and a fifth, which is the separation (S) of the peak of the flanking subregion from the peak of the centre subregion. Thus nine parameters would be sufficient to describe an odd-symmetric receptive field composed of two subregions as shown in figure 2*b*.

Rather than adding a further set of five parameters to describe a receptive field with three subregions, as in figure 2*a*, we constrained the model so that both flanking subregions had the same spatial properties. With this constraint, the introduction of a symmetry parameter (g) allows a description of the full range of behaviour from pure even symmetry to pure odd symmetry as illustrated in figure 1. When $g = 0.0$, the model has only one flanking subregion. When $g = 0.5$, the model depicts a receptive field with two identical flanking subregions. When $g = 0.25$, there are two flanking subregions with identical space constants, but the amplitude of one is greater than the other in a ratio of 2:1.

For a purely bandpass spatial-contrast sensitivity function, with no response at all below a certain low spatial frequency, the sensitivity of the central subregion ($k_{c_1} - k_{s_1}$) minus the sensitivity of the flanking subregions ($k_{c_2} - k_{s_2}$) should be zero (i.e. the centre and the flanks of the receptive field should be balanced.) On the other hand, for a bandpass spatial contrast sensitivity function with a significant lowpass component, ($k_{c_1} - k_{s_1}$) will be greater than ($k_{c_2} - k_{s_2}$). Because most neurons show bandpass spatial-contrast sensitivity functions, without a large lowpass component, we imposed a final constraint on this model such that the combined sensitivity of all subregions summed to zero. This means that the receptive field should give zero response to changes in the overall illumination level. This has the advantage of reducing the number of free parameters in the model from ten to nine (see Appendix, equation (A1)). For a cell with a significant lowpass component in the spatial-contrast sensitivity function, the model obviously should not be constrained in this manner.

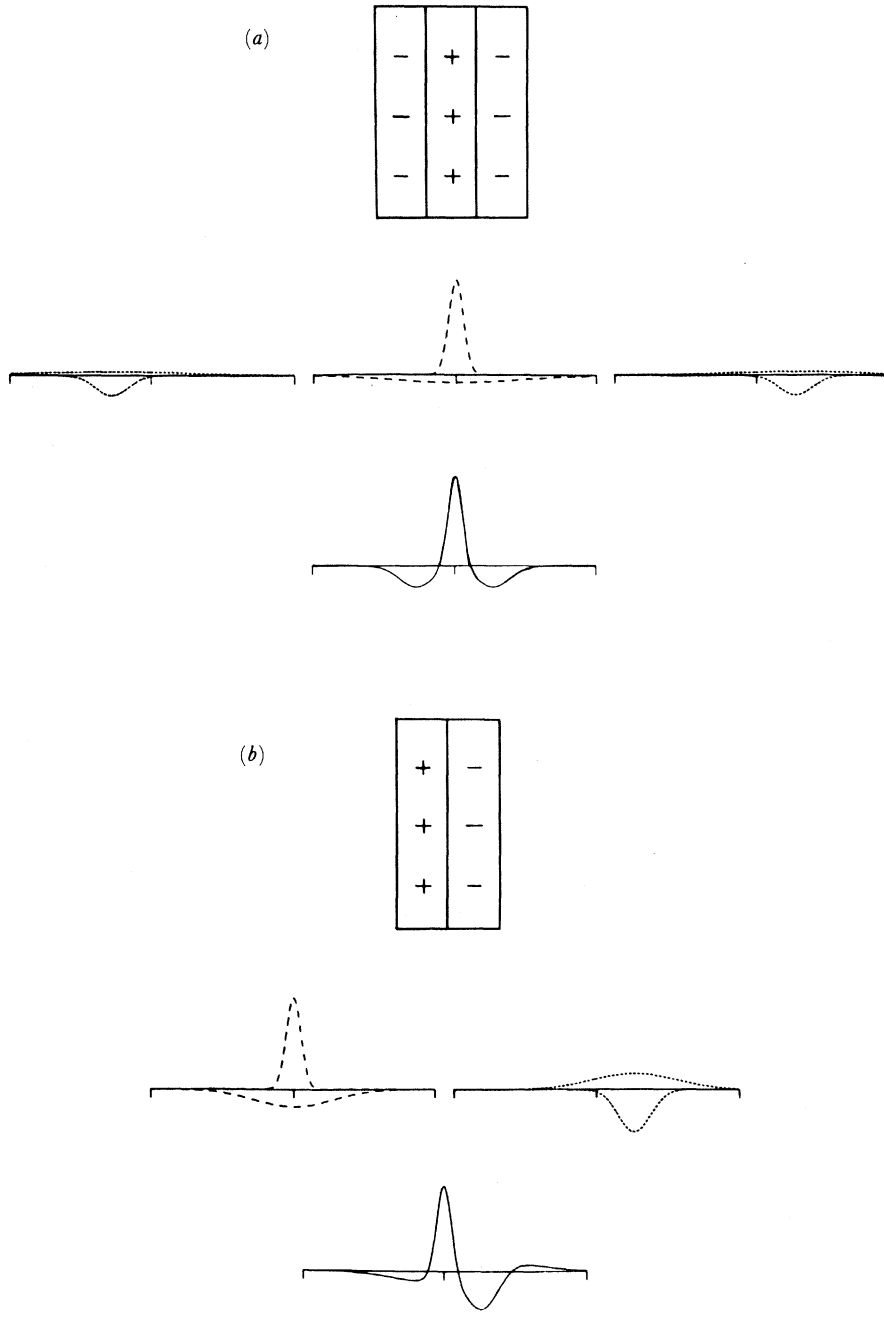

FIGURE 2. For description see opposite.

We have called this model, with nine parameters, d-DOG-s (the difference of the difference of Gaussians with separation). Although the choice of parameters almost certainly under-represents the actual one-dimensional organization of the receptive field, even this large number of parameters makes the model complicated and difficult to test. Fortunately, the d-DOG-s model can be well approximated by functions that are subsets of this model and have a reduced number of parameters:

(i) *The simple DOG model.* In this case the cortical receptive field is modelled with a single DOG function, specified by four parameters: the space constant (x_c) and amplitude (k_c) of the centre Gaussian and the space constant (x_s) and amplitude (k_s) of the surround Gaussian, where the peaks of the centre and surround space constants are spatially coincident (see Appendix, equation (A 3)). In this simplified model, the flanking subregions of the receptive field are formed by the extremities of the surround Gaussian because of the difference in spatial extent of the centre and surround components. This is the minimal version of the d-DOG-s model that retains the spatial bandpass characteristic required to model cortical cells. It is also easy to compare quantitatively with the Gabor model because they both have four parameters (see figure 14). The DOG has been proposed previously as the basis of a model of cortical neurons (Rose 1979). An example of the hand-plotted receptive field, the component Gaussians and the resultant spatial weighting function of the difference of two Gaussians is illustrated in figure 3*a*. In the form used here, this model is always of even-symmetric form.

(ii) *The DOG-s model.* To test the importance of the parameter (S) that specifies the separation of the peaks of the centre and flanking subregions of the receptive field, we stripped as many parameters as possible from the d-DOG-s model while retaining the characteristic behaviour associated with the separation parameter. This resulted in the DOG-s model, which is the even-symmetric form of the d-DOG-s model with only the centre components of each DOG ($x_{c_1}, k_{c_1}, x_{c_2}, k_{c_2}$) and the separation parameter (S) retained (see Appendix, equation (A 2)). Figure 3*b* shows that this leaves three Gaussian mechanisms, where each subregion of the receptive

---

FIGURE 2. Schematic representation of the individual Gaussian components and their combination for a receptive-field model based on the difference of difference-of-Gaussians with separation (d-DOG-s, equation A 1). Each subregion of a receptive field is described by a difference-of-Gaussians function. Thus for a purely even-symmetric field, with three subregions, there are six Gaussians altogether. For an odd-symmetric field, with two subregions, there are only four Gaussians. (*a*) Purely even-symmetric field. The upper row shows an idealized 'hand-plotted' receptive field, with 'on' centre (+) and 'off' surround (−) subregions. The second row illustrates the individual Gaussians of each of the DOGs that make up the subregions of the d-DOG-s. The third row gives the spatial weighting function of the receptive field based on the linear combination of the three DOGs in the second row. (*b*) Odd-symmetric receptive field. The upper row shows the hand-plotted receptive field with 'on' and 'off' subregions. The second row shows the individual Gaussians that make up the DOGs corresponding to the 'on' and the 'off' subregions in the upper row. The third row shows the form of the spatial weighting function that is the resultant of the two DOGs in the second row. It should be noted that the individual Gaussians of the 'on' and 'off' subregions do not necessarily have the same space constants and sensitivities. Consequently the resulting function, shown in the bottom row, need not be exactly odd-symmetric.

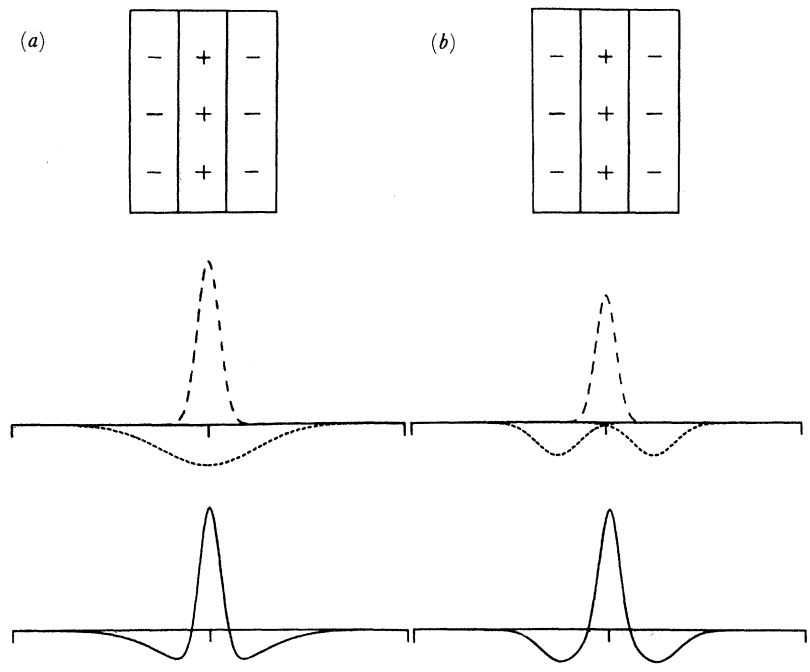

FIGURE 3. (*a*) Schematic representation of the difference-of-Gaussians (DOG, equation A 3), where the peaks of the two Gaussians are spatially coincident. In this case the flanking subregions of the receptive field are formed by the spatial extremities of the surround Gaussian. The first row is the hand-plotted receptive field, the second row shows the component Gaussians of the centre ('on') region and the surround ('off') regions, and the third row gives the spatial weighting function based on the linear combination of the Gaussians in the second row. (*b*) Representation of the difference-of-Gaussians with separation (DOG-S, equation A 2). The three rows are in the same sequence as described above for (*a*). This is equivalent to the purely even-symmetric version of the d-DOG-S model, where each subregion is modelled by a single Gaussian rather than a DOG.

field is served by a single Gaussian. The two Gaussians specifying the flanking subregions were constrained to have the same space constants and sensitivity parameters. This constraint is similar to that applied to the d-DOG-S model. To the extent that the surrounds of LGN neurons are weak, particularly in the parvocellular layers, the DOG-S model (which simply lacks the components due to these LGN surrounds) retains the significant features of the general case.

This function reduces to the simple DOG when the separation parameter is zero. Indeed the DOG-S model can be considered as a rearranged version of the DOG model, where the surround has been split into two Gaussians and the peaks of the two halves have been relocated at distances $+S$ and $-S$ from the peak of the centre mechanism (figure 3*b*). For this reason, the notation of the DOG model has been followed in describing the DOG-S model and the parameters of the flanking regions are therefore designated by k_s for sensitivity and x_s for the space constant. On the other hand, in terms of the d-DOG-S model, these parameters associated with the flanking subregions would be k_{c_2} and x_{c_2}.

The subunits of the DOG models can most easily be considered as derived from individual geniculate cells with a centre–surround receptive-field organization. To preserve the relations between the values of the space constants and amplitudes of the centre and surround mechanisms of LGN neurons and those obtained from the fitting of DOG models to the cortical data, bounds were imposed on the parameters during the fitting procedure. Thus the peak contrast sensitivity and space constant of the centre mechanism were constrained to be within the bounds of values found for geniculate neurons (Kaplan & Shapley 1982; Derrington & Lennie 1984). Most often the choice of parameter values to give the best-fitting function did not reach the bounding constraints because the selected values fell naturally in the range found for geniculate cells. Of course, the imposition of constraints on a parameter puts the constrained version of a model at a disadvantage with respect to the unconstrained version. However, in the case of the DOG-based models, this disadvantage is outweighed by the fact that the parameter values can be given a direct functional interpretation (see Discussion).

The Gabor model

The Gabor function has been proposed as a model for the receptive-field profiles of simple cells (Marčelja 1980; Kulikowski *et al.* 1982; Daugman 1985; Field & Tolhurst 1986), and for psychophysically defined channels (Watson 1983; Daugman 1984). If one wishes to represent an image in terms of space and spatial frequency, the Gabor representation is optimal in terms of compactness, minimizing the uncertainty associated with localizing a signal simultaneously in space and spatial frequency. This fact has been considered to be of potential significance for the efficient processing of visual information (Marčelja 1980; Daugman 1984, 1985). The function is the product of a sinusoid with a single Gaussian envelope (see Appendix, equation (A 4)) and is defined by four parameters: the space constant of the Gaussian (x_c) and its amplitude (k_c), the frequency of the sinusoid (f_c) and the phase of the sinusoid (p) with respect to the Gaussian. Spatial weighting profiles given by this function, for two cells, are shown in figure 9 (a, b) and can be seen to have roughly the shape required for the hypothetical spatial weighting of a bandpass filter shown in figure 1.

The differential-of-Gaussian model

The Laplacian of a Gaussian ($\nabla^2 G$) was introduced by Marr & Hildreth (1980) as a model of the concentrically organized receptive fields of retinal ganglion cells, to support a representation of the image based on zero-crossings. We have considered a one-dimensional version of this, the second differential of a Gaussian (D^2G), as a model of cortical cells. This function has two parameters, the space constant of the Gaussian (x_c) and a scaling constant (k_c) (see equation (A 5)). Figure 10 (a, b) illustrates two examples of the spatial weighting profile. A particular constraint imposed by this function is that the low-frequency portion of the predicted spatial-frequency tuning function is a straight line with a slope of two in logarithmic coordinates. Marr & Hildreth (1980) pointed out that the Laplacian of a Gaussian can be approximated by a circularly symmetric DOG function, provided that the ratio of the surround space constant to the centre space constant

is 1.6:1 or smaller. Such a relation would also clearly be true for the D^2G model and the DOG model discussed earlier. It is important to appreciate that the DOG function is equivalent to D^2G only if this constraint applies. In the results presented here applying this constraint would result in the mistaken conclusion that the DOG model is a poor description of the spatial-contrast sensitivity functions because the ratio of surround to centre space constants is seldom less than two.

We have also considered a model composed of two D^2G functions of opposite sign, spatially separated by $2x_c$, since this function has been given prominence as a specific model for simple cells in computational theories of vision (Marr & Hildreth 1980; Marr & Ullman 1981; Marr 1982). This model, however, produced even less satisfactory fits to the spatial-contrast sensitivity functions than the D^2G function, so the detailed results have not been included.

METHODS

Physiological experiments were performed on eight adult Old World monkeys (7 *Macaca fascicularis* and 1 *Cercopithicus aethiops*) weighing between 3.3 and 5.5 kg.

Preparation

Animals were anaesthetized with intramuscular ketamine for venous cannulation and then maintained on intravenous steroid anaesthetic (Saffan) for the ensuing surgery. All incisions were infiltrated with long-lasting local anaesthetic (Marcain) and any pressure points were treated with topical anaesthetic (Tronothane). For recording, animals were anaesthetized with barbiturate (Sagatal; 6 mg kg^{-1}), and paralysed with pancuronium bromide (Pavulon; 0.2 mg kg^{-1}); then both the anaesthetic (Sagatal; 1.2–3.0 mg kg^{-1} h^{-1}) and muscle relaxant (Pavulon; 0.2 mg kg^{-1} h^{-1}) were continuously infused intravenously, in a solution of 10% (by mass) glucose in 0.9% (by mass) NaCl at 5.6 ml h^{-1}, to maintain anaesthesia and paralysis. The electrocardiogram (ECG) and electroencephalogram (EEG) were monitored continuously and the anaesthetic state was judged to be satisfactory if there was almost continuous slow-wave EEG activity and if mildly noxious stimuli produced no change in EEG or heart rate. Supplementary anaesthetic doses were administered, if necessary, to maintain the anaesthetic state. Animals were artificially hyperventilated with room air to which CO_2 was added to maintain end-expiratory CO_2 at 4.5–5.5%. Rectal temperature was monitored continuously and maintained at 37.5–38 °C.

The pupils were dilated by topical application of atropine sulphate and zero-power contact lenses were fitted to protect each cornea. The animal viewed the visual display through 3 mm artificial pupils and additional spherical correcting lenses. The refractive state of each eye was initially judged by direct ophthalmoscopy and further checked at intervals throughout the experiment by determining the highest spatial frequency that evoked a response just greater than the background firing of a neuron and adjusting the lenses if necessary.

Recording

Glass-coated tungsten microelectrodes (Merrill & Ainsworth 1972) with 4–8 μm exposed tips were lowered to the cortical surface, through a small craniotomy and durotomy, under visual control and the exposure was sealed with 2 % agar in 0.9 % saline. The whole area was covered with a mixture of paraffin oil and Vaseline to prevent drying. Action potentials were amplified and the individual spikes of well-isolated neurons selected by a level discriminator that triggered a standard TTL pulse as output to a computer. Successive traces of the recording were superimposed on a storage oscilloscope triggered by the level discriminator, to allow monitoring of the waveform of the action potential and to assess whether the recording was from a single cell.

Visual stimuli

Receptive fields were plotted by hand with lines, bars or spots back-projected on a tangent screen 171 cm from the animal. The projections of the foveae were marked on the tangent screen by using an ophthalmoscope with a reversing prism (Eldridge 1979); repeated determinations of the projection of the same retinal position were always within 0.5° and most often 0.25° or less. From the hand plots of receptive fields we determined the eccentricity, an initial classification of cell type (simple or complex), the ocular dominance (Hubel & Wiesel 1962) and some indication of the colour preference by using broad-band Wratten filters. The 'simple' or 'complex' categorization was further analysed, quantitatively, by using a test of linearity of spatial summation. For quantitative assessment of responses to visual stimuli, gratings varying sinusoidally in luminance profile were displayed on a cathode-ray tube (Joyce Electronics), 30 cm × 22 cm with a white (P4) phosphor (luminance: 280 cd m^{-2}), positioned 342 or 456 cm in front of the animal. The bars of the grating could be restricted in height, to produce a strip of grating flanked by uniform areas of the same mean luminance, so as to optimize the stimulation conditions for cells with end-stopped receptive fields (Hubel & Wiesel 1965; Bishop *et al.* 1971; Gilbert 1977), for which elongated bars were relatively ineffective.

Measurement of response properties

Spatial-frequency response tuning

The magnitude of the response to a range of spatial frequencies presented in pseudo-random order at a contrast of 0.7 was measured for between 10 and 20 presentations of each stimulus sequence, consisting of at least two cycles of a drifting grating. The orientation, drift rate and direction of motion were optimized by listening to the responses before the tuning function was determined.

Orientation tuning

The response of the unit was determined at a number of orientations for both directions of drift; the steps in orientation varied between 2.5° for the most sharply tuned cells and 20° for cells with little or no preference for orientation. The spatial

frequency of the grating used was that which gave the largest response during measurement of spatial frequency tuning and the contrast was always 0.7. Each stimulus was presented between 5 and 20 times in pseudo-random order.

Spatial summation

The response to stationary, contrast-modulated gratings was determined at 12 phase angles, covering 360° (the dimension of one full cycle of the grating) in 30° steps. Each phase was presented for two temporal cycles, the contrast being modulated sinusoidally between −0.7 and +0.7 at the optimal temporal frequency for the cell. Each stimulus was presented 10–20 times with all phases selected in a pseudo-random order. During the analysis of data after the experiment, we determined the spatial frequency at the peak of the response function. Because there are some cortical cells that appear to be predominantly linear at low spatial frequencies but nonlinear at high spatial frequencies (Movshon *et al.* 1978*a*, *b*), only those cells for which the spatial frequency of the test grating on the summation test was 0.7 times the peak spatial frequency or greater are included here.

Contrast sensitivity

To determine the contrast sensitivity of neurons, we used a staircase method similar to that described by Derrington & Lennie (1982). For gratings of various spatial frequencies covering the range over which the cell responded (determined from the spatial-frequency response tuning) we measured the contrast sensitivity of the cell by using this staircase method. Initially, the mean and the variance of the background discharge of the cell were determined, with the receptive field of the cell centred on the display with no grating present. The mean was calculated over 16 periods, each period equal in duration to the period for which the grating stimulus would be presented. Then a drifting grating was presented (without change in mean luminance) and the spikes elicited during the presentation were accumulated, discounting the duration corresponding to the first half-cycle of the grating to avoid temporal transients. After this there was a pause, equal to the presentation time of the grating, then a further period during which another single measurement of the background firing was made, before the next grating was displayed. An online running estimate of the mean and variance of the background was determined by using the values collected in the 16 most recent periods of measurement. After the presentation of each stimulus, the number of spikes occurring during that particular trial was compared with a statistical criterion (two standard deviations greater than the background mean for these experiments). If the evoked response exceeded the criterion, the contrast was reduced on the next trial at that particular spatial frequency; if not, the contrast was increased. The staircase was run at each spatial frequency until the computer had accumulated at least 8 reversals (in later experiments, 24 reversals) at a step size of 0.0125 log unit, or until there was no response greater than the criterion at the highest possible contrast (0.7). The order of presentation of spatial frequency was chosen randomly by the computer. Using this method, we could obtain a complete spatial-contrast sensitivity function for each cell at its optimal orientation. This took between 15 and 45 min, depending on the number of spatial frequencies, the rate of convergence of the staircase and the other stimulus parameters.

For all measures, other than the staircase determination of contrast sensitivity, the computer accumulated online peristimulus time histograms (PSTHS) for each stimulus condition and for a blank period. In addition the total number of spikes elicited on each stimulus presentation was stored along with an estimate of the magnitude of the fundamental component of the response, at the temporal frequency of the drifting grating (Derrington & Lennie 1982).

Histology

The position of the tip of the electrode was marked at regular intervals by making small electrolytic lesions (2–3 μA for 2–3 s, tip negative). At the end of the experiment the animal was killed with an overdose of anaesthetic. The methods used in perfusion, histological reconstruction of penetrations and assignment of laminar position for each cell have been described previously (Hawken & Parker 1984).

RESULTS

Cell classification

Some cells could be clearly classified as simple: the hand plot of their receptive fields revealed spatially segregated 'on' and 'off' subregions that were mutually opponent; on the test of spatial summation, they produced modulated responses in phase with the temporal modulation of the stimulus at some spatial phases, while showing clear null positions (no response despite modulation of the grating) at $\frac{1}{2}\pi$ radians from the phase that gave the biggest response; with drifting sinewave gratings, the responses at all spatial frequencies were strongly modulated at the temporal frequency of the stimulus.

Other cells showed all the characteristics of classical complex cells: they gave 'on/off' responses at all positions in their receptive fields to a flashing bar; they produced a clear second harmonic response at all spatial phases on the test of linearity of spatial summation; with drifting gratings, they showed little or no response modulation at the temporal frequency of the stimulus but responded with an increase in the mean discharge. However, there were cells that did not fall clearly into either of these categories. For example, some cells, which in most respects appeared simple, gave an indication of a second harmonic response at the expected null position, especially for spatial frequencies on the high-frequency limb of the spatial-frequency tuning function. But these cells showed modulated responses to drifting grating stimuli. Although some of the anomalies could be attributed to slow drifts of the eyes or pulsations due to cardiovascular or respiratory movements, experience in the cat, where the receptive fields are larger and these mechanical problems not so severe, suggests that there are cells that genuinely show a mixture of linear and nonlinear behaviour at many spatial frequencies.

To obtain a quantitative indication of the degree of linearity of spatial summation, the response of each cell was determined, for a set of spatial phases covering the full 2π radians of phase angle in steps of $\frac{1}{6}\pi$ radians. The details of the test are presented in the Methods section. For retinal ganglion cells and for lateral geniculate neurons, the ratio of the mean of the second harmonic responses

(f_2) to the peak amplitude of the fundamental response (f_1) has been used as an index of linearity of spatial summation (Hochstein & Shapley 1976; Derrington & Lennie 1984).

Figure 4 shows that the distribution of f_2/f_1 ratios is weakly bimodal for the total sample of cortical cells (cf. Dean & Tolhurst 1983). DeValois *et al.* (1982) used the

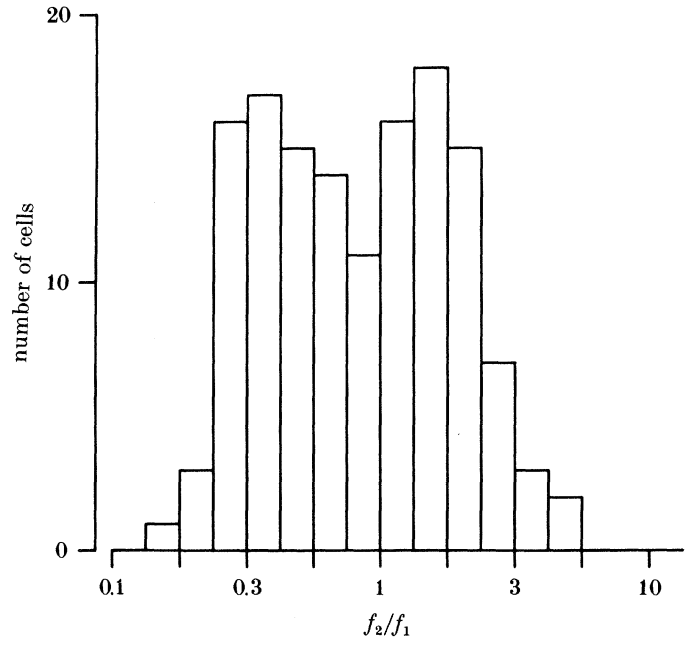

FIGURE 4. The distribution of 138 neurons on a test of the linearity of spatial summation. The receptive field of each neuron was stimulated with a temporally modulated sinewave grating at 12 different spatial phases. The amplitude of the second harmonic component of the impulse discharge (at twice the frequency of the temporal modulation) was averaged over all spatial phases to give the value f_2. The value of f_1 was determined at the spatial phase that gave the greatest fundamental response at the same frequency as the temporal modulation. Cells with f_2/f_1 ratios of less than unity were considered to have a dominant linear component and have been classified as simple (77 cells); those with f_2/f_1 ratios greater than unity, showing a dominant nonlinear response, have been classified as complex (61 cells).

ratio of the fundamental to DC response (f_1/f_0) for drifting gratings to classify cells in the macaque striate cortex. They found a more clearly bimodal distribution of the f_1/f_0 ratio and distinguished their population on the basis of this test. In this paper, simple cells have been classified as those with a f_2/f_1 ratio less than one for stationary modulated gratings, which indicates that the fundamental component dominates over the second harmonic. Complex cells have been classified as those with f_2/f_1 ratios of greater than one, which indicates a dominant non-linear component. Based on the f_2/f_1 index, we have 77 simple and 61 complex cells. These percentages of simple and complex cells based on the f_2/f_1 index are very similar to those found by DeValois *et al.* (1982); this result is to be expected since both the tests define simple cells as those having a prominent f_1 component.

Measurements of contrast sensitivity

For each cell, the measurement of contrast sensitivity was obtained at spatial frequencies of about one third of an octave apart, by means of the staircase procedure described in the Methods. To determine the correct transformation of the data to use in fitting the curves to the data by the method of least squares, the relation between the mean and variance of the contrast-sensitivity measurements was investigated. In three of the eight animals, we collected 24 reversals (rather than the normal 8) on the staircase measure of contrast sensitivity. This gives 12 independent measures of threshold at each spatial frequency and from these the variance of the mean contrast threshold was estimated (Wetherill & Levitt 1965). There is a clear positive relation between the arithmetic mean and variance of linear contrast values (variance = $k \times \text{mean}^{1.85}$) (see figure 5). Because the exponent of the power function relating the mean and variance was almost two, a

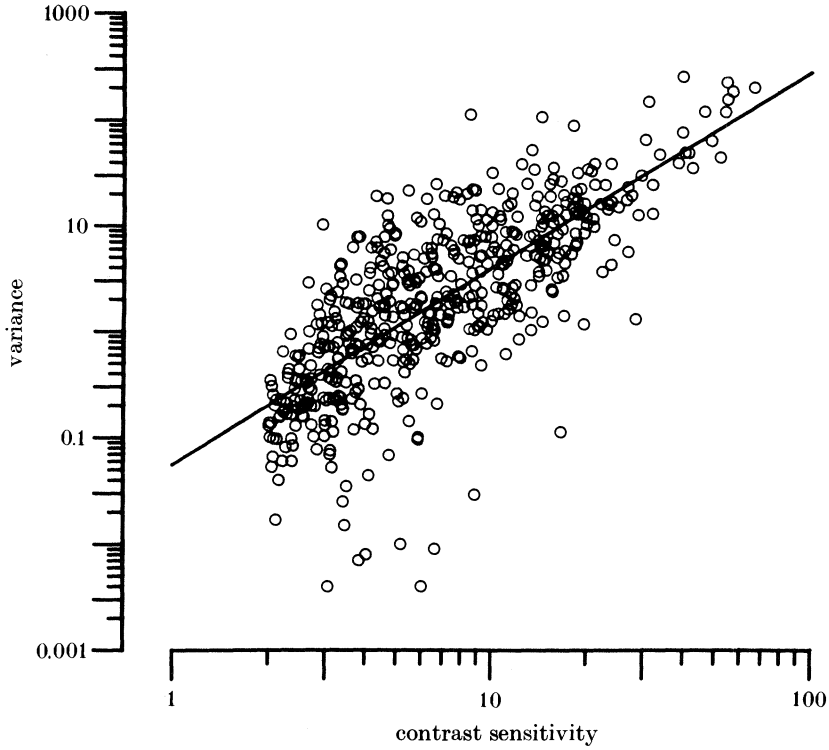

FIGURE 5. Relation between mean contrast sensitivity and variance of measures of contrast sensitivity. The mean value of contrast sensitivity and the associated variance were obtained from 12 estimates obtained by using the staircase procedure described in the Methods section. For each cell, the mean and variance were calculated at every spatial frequency that yielded a significant response. Initially, the calculations were based on the assumption of a linear contrast scale (arithmetic mean and variance). The figure shows all these measurements pooled together. There is a positive relation between arithmetic mean and variance with a slope of 1.85 as indicated by the solid line on the graph. A slope of 2 would indicate equal variance for logarithmically transformed values of contrast sensitivity.

logarithmic transformation of the contrast-sensitivity values was taken to make the data homoscedastic. For models specified in equations (A 1)–(A 4) (see Appendix) a general-purpose minimization routine (STEPIT) was used to find the best-fitting functions, whereas a logarithmic transformation makes equation (A 5) linear, so for this model the best fit was obtained by direct solution of the normal equation.

Evaluation of models

In each figure that shows contrast sensitivity as a function of spatial frequency (e.g. figure 6) the mean contrast sensitivity at each spatial frequency is shown by the open circles (± one s.d.). The contrast-sensitivity measurements obtained for

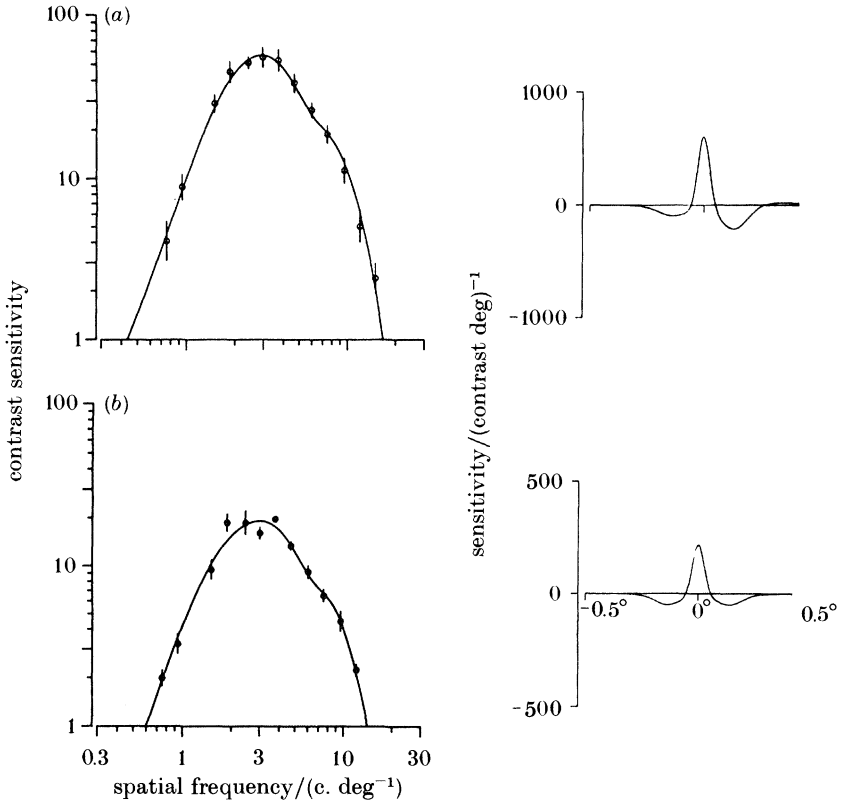

FIGURE 6. The d-DOG-s model (equation A 1) fitted to the contrast-sensitivity functions (left) of two simple cells. The derived spatial weighting functions are shown on the right. Each determination of contrast sensitivity (circles) is the mean of 12 estimates from a staircase procedure; the error bars indicate +/− one standard deviation from the mean. The neuron whose sensitivity function is shown in (*a*) was recorded in layer VI of the striate cortex; the centre of the receptive field was located 1.2 degrees from the fovea. The neuron whose sensitivity function is shown in (*b*) was recorded in layer II in the same penetration. The values of the parameters of the best-fitting function are: (*a*), $A_1 = 43$, $A_2 = 43$, $A_3 = 41$, $A_4 = 41$, $x_{c_1} = 2.22'$, $x_{s_1} = 15.36'$, $x_{c_2} = 4.97'$, $x_{s_2} = 17.41'$, $g = 0.25$, $S = 8.23'$; (*b*), $A_1 = 16$, $A_2 = 16$, $A_3 = 10$, $A_4 = 10$, $x_{c_1} = 2.23'$, $x_{s_1} = 16.10'$, $x_{c_2} = 4.41'$, $x_{s_2} = 27.46'$, $g = 0.5$, $S = 8.29'$.

two simple cells are shown in the left panels of figures 6–10, with the smooth curves being the best-fitting versions of the amplitude spectra of the models: d-DOG-s (figure 6*a*, *b*), DOG-s (figure 7*a*, *b*), DOG (figure 8*a*, *b*), Gabor (figure 9*a*, *b*) and D^2G (figure 10*a*, *b*). The two examples were chosen because they had relatively high sensitivities (allowing the models to be discriminated from one another), had

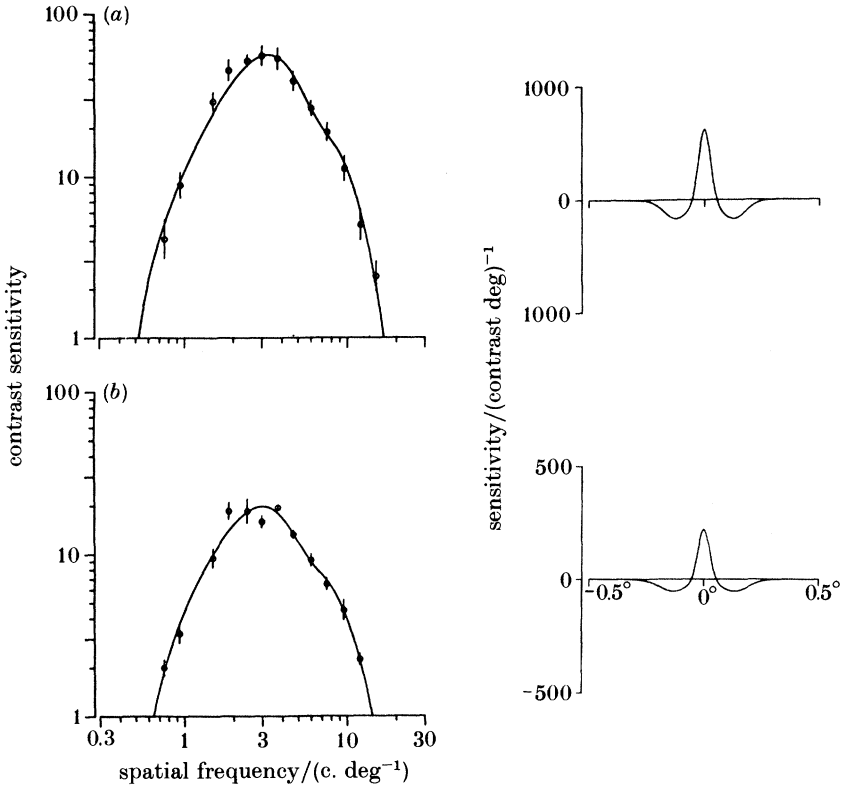

FIGURE 7. The DOG-s model (equation A 2) fitted to the contrast sensitivity functions of the same two cells as shown in figure 6. The details of the procedure and of the cells are given in figure 6. The values of the parameters of the best-fitting function are: (*a*), $B_1 = 42.1$, $B_2 = 45.2$, $x_c = 2.21'$, $x_s = 4.58'$, $S = 7.38'$; (*b*), $B_1 = 15.0$, $B_2 = 16.6$, $x_c = 2.19'$, $x_s = 5.25'$, $S = 7.92'$.

intermediate bandwidths for our sample of cells, came from different laminae in the region of the cortex devoted to foveal vision, and showed relatively low variance over the data points (again allowing the models to be most readily discriminated). Figure 13 shows a wider variety of sensitivity functions, including some of the most extreme forms. The two examples are shown in each of the five figures (6–10). The right hand panel shows the spatial weighting function associated with the sensitivity function shown in the corresponding left-hand panel.

For each model the parameters were chosen so that they minimized

$$\sum_i [\lg(\text{model}) - \lg(\text{data})]^2.$$

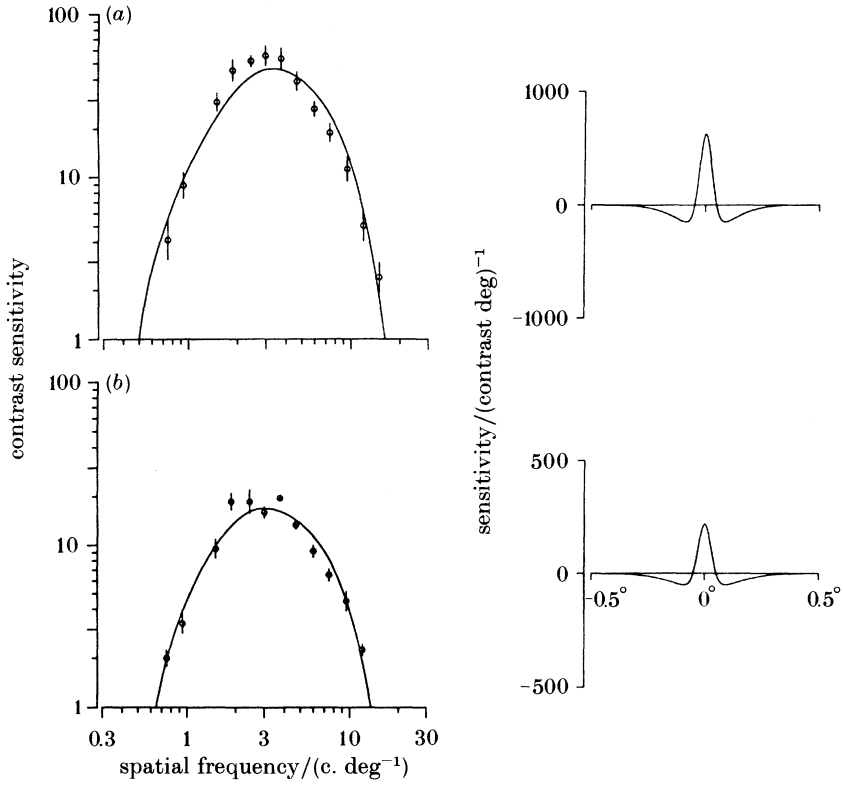

FIGURE 8. The DOG model (equation A 3) fitted to the contrast-sensitivity functions of the same two cells as shown in figure 6. The details of the procedure and of the cells are given in figure 6. The values of the parameters of the best-fitting function are: (*a*), $C_1 = 58.5$, $C_2 = 61.4$, $x_c = 2.38'$, $x_s = 10.14'$; (*b*), $C_1 = 20.7$, $C_2 = 22.8$, $x_c = 2.45'$, $x_s = 11.54'$.

To provide an estimate of the deviation between the measured values of contrast sensitivity and the best-fitting function from each model, the above quantity was divided by the number of data points to give the mean error per data point (Linsenmeier *et al.* 1982). The mean error allows a comparison between cells with different numbers of values making up the spatial-contrast sensitivity function. For the cell whose sensitivity function is illustrated in the top of figures 6–10, the mean error for the best-fitting version of each model is given in table 1*a*; the error associated with each model for the cell illustrated in the lower half of figures 6–10 is given in table 1*b*.

Both on visual inspection of the fits to the spatial-contrast sensitivity functions and in terms of the mean error per data point, models based on the difference-of-Gaussians provide a much more accurate description of the spatial tuning than do the Gabor or the second differential of a Gaussian. An *F*-test for lack of fit of a model, based on the standard procedures for linear regression, can be obtained by comparing the estimates of variance measured during the experiment with the residual sum-of-squares deviation of the fitted function from the data. Unfortun-

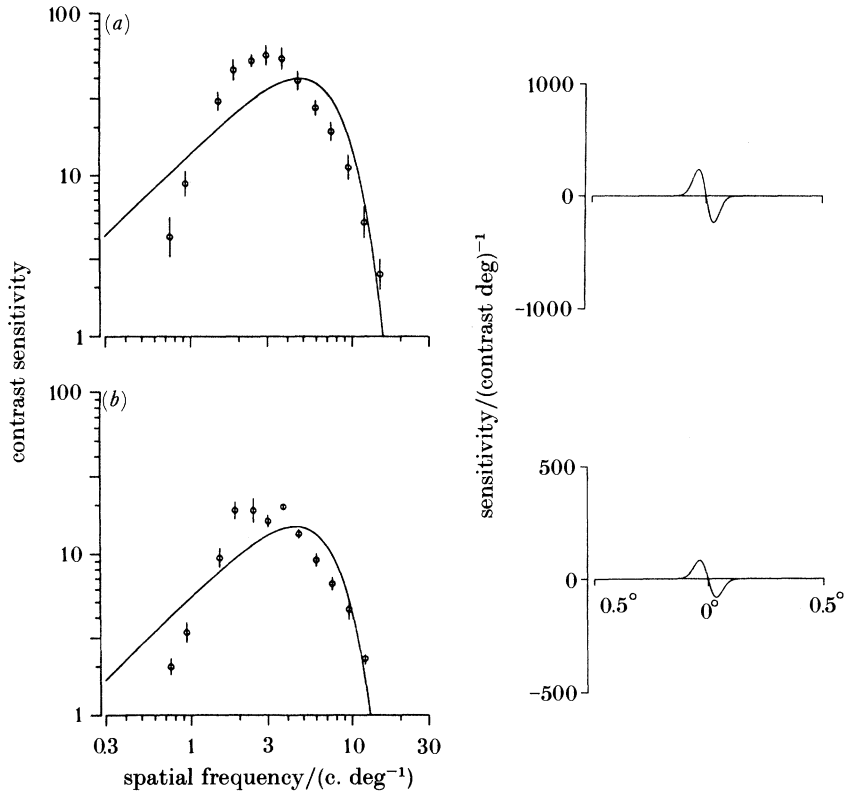

FIGURE 9. The Gabor model (equation A 4) fitted to the contrast-sensitivity functions of the same two cells as shown in figure 6. In almost all cases, the observed functions were more nearly symmetrical than the Gabor function plotted on logarithmic axes. The details of the procedure and of the cells are given in figure 6. The values of the parameters of the best-fitting function are: (*a*), $D_1 = 41.8, x_c = 1.94', f_c = 2.92$ c. deg$^{-1}, p = 90°$; (*b*), $D_1 = 23.8$, $x_c = 2.04', f_c = 3.16$ c deg^{-1}, $p = 90°$.

ately, this procedure is only exactly valid for models that can be made linear in their parameters, such as D^2G. It is not well established that the other four models can be treated in this way, because they are nonlinear in their parameters. Nonetheless, although the exact values of F-ratios should be interpreted conservatively, they do provide a useful measure of comparative performance (Draper & Smith 1966, pp. 282 and 299). With the number of degrees of freedom for the data in table 1, even F-ratios as small as 6 would be associated with a significance level of less than 0.001. All the firm conclusions we wish to draw concerning these models are supported by F-ratios of 60 or greater.

The results of the F-ratio test are clear for D^2G, which is linear in its parameters: both cells in figure 10 show significant *lack* of fit (see table 1). The values of the F-ratio for the Gabor model (figure 9) are also very large. Thus, both these models can be confidently rejected.

Two aspects of the inability of the Gabor and D^2G functions to match the shape

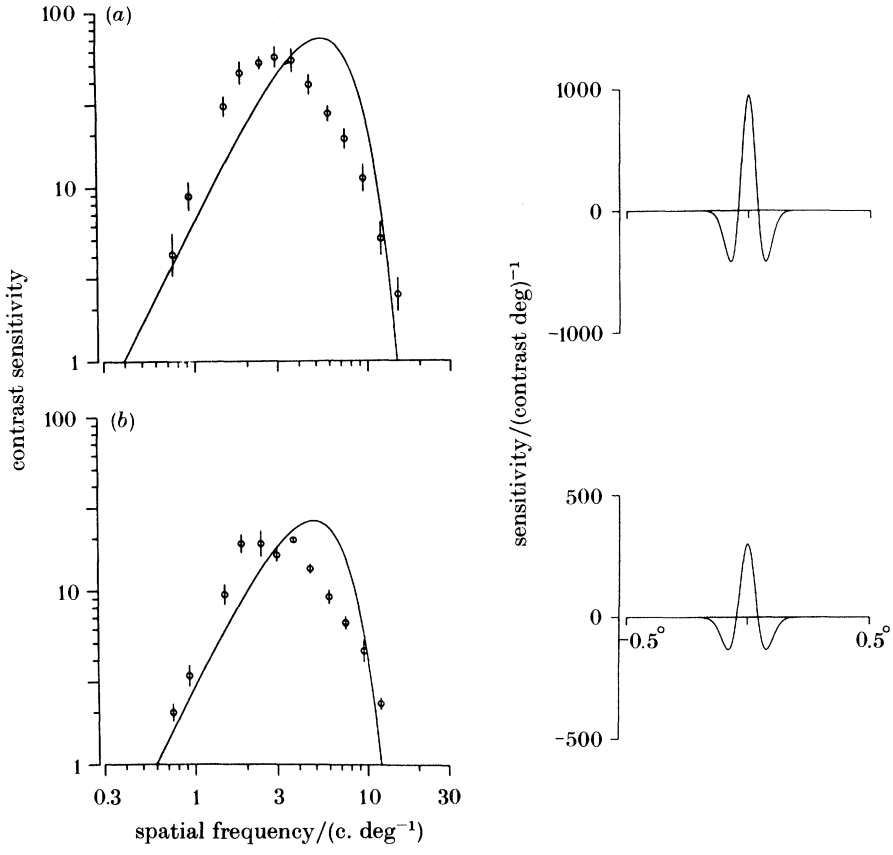

FIGURE 10. The D^2G model (equation A 5) fitted to the contrast-sensitivity functions of the same two cells as shown in figure 6. Like the Gabor function (figure 9), D^2G is not as symmetric as the data on logarithmic axes. The details of the procedure and of the cells are given in figure 6. The values of the parameters of the best-fitting function are: (*a*), $E_1 = 6.48$, $x_c = 3.49'$; (*b*), $E_1 = 2.87$, $x_c = 3.90'$.

demanded by the data points in figures 9 and 10 are particularly striking. First, the low-frequency limb of the tuning curve is poorly described. Second, a consequence of the attempt by the fitting procedure to accommodate the low-frequency limb is that the peak spatial frequency of the model functions is far removed from the peak defined by the data (half to one octave too high). The attempt to fit the low-frequency limb of the tuning curve also explains why the fitting procedure arrived at a purely odd-symmetric version of the Gabor function. Any purely odd-symmetric receptive field necessarily has zero response at zero spatial frequency. Hence selection of the odd-symmetric version of the model by the fitting procedure allows the steepest possible low-frequency roll-off in the amplitude spectrum, but even this choice is inadequate.

The DOG-S and DOG models differ only in the inclusion of a separation parameter (S) for the DOG-S model. This parameter is an additional complication but has some particularly attractive interpretations in terms of receptive-field organization and

TABLE 1. THE MEAN ERROR PER DATA POINT AND F-RATIO FOR THE BEST-FITTING VERSION OF EACH MODEL TO THE SPATIAL-CONTRAST SENSITIVITY FUNCTIONS SHOWN IN FIGURES 6–10

	d-DOG-S	DOG-S	DOG	Gabor	D^2G
(*a*)					
error	0.0013	0.0032	0.0097	0.0448	0.0933
F-ratio	4.5	4.69	12.5	60.6	94.9
	(4,134)	(8,134)	(9,134)	(9,134)	(11,134)
(*b*)					
error	0.0018	0.0025	0.0053	0.0312	0.0591
F-ratio	15.7	9.3	17.4	84.7	152.7
	(3,124)	(7,124)	(8,124)	(8,124)	(10,124)

its possible anatomical substrate (see Discussion), so it is important to assess quantitatively the case for its inclusion. A partial F-test (Draper & Smith 1966, pp. 67–72) can be applied to examine whether a particular parameter significantly improves the fit of a model. The F-ratio is again very large: $F(1, 134) = 74.8$ for the cell in the upper half of figures 6–10, $F(1, 124) = 74.1$ for the cell in the lower half of figures 6–10. These results argue strongly for the inclusion of the separation parameter.

Spatial weighting functions

Each model and its parameters has associated with it a characteristic spatial weighting function. Because the spatial-contrast sensitivity measurements that define the amplitude spectra place quite strong constraints on the shape of the best-fitting function and the parameter values associated with the function, it is informative to compare the shapes of the spatial weighting functions derived from each of the models. The right-hand columns in figures 6–10 show the associated spatial weighting functions for each of the amplitude spectra in the left-hand column. Although these weighting functions were not derived from independent experimental measures, the difference in their shapes illustrates how the choice of a DOG-based model, as opposed to a Gabor function or second differential of a Gaussian, would result in different predictions for the spatial organization of the receptive field.

A second important feature of the spatial weighting functions is that they show that some parameters of the receptive field are robustly defined. The space constants of the centre Gaussian mechanisms for the three DOG-based models applied to the contrast-sensitivity function of the cell, shown in the upper half of the figures 6–8, are almost identical (2.22′, 2.21′, 2.38′ for d-DOG-S, DOG-S and DOG respectively); a similar close correspondence holds for the cell in the lower half of each of these figures (2.23′, 2.19′, 2.45′). In the case of DOG-S, which we have argued is a very reasonable approximation to d-DOG-S, those parameters that are common to both models have values that are within 20 %, for the two cells in figures 6 and 7. The DOG-based models also allow realistic comparisons to be made between cells in the striate cortex and those in the lateral geniculate nucleus. In general, the sensitivities and space constants of the centre mechanisms of cortical cells derived

from the DOG-based models fall very nicely in the range of values found for the centre mechanisms of neurons in the LGN (Derrington & Lennie 1984).

Comparison between models for the entire sample of neurons

Figure 11 shows the mean error per data point plotted against the variance per data point, also calculated on logarithmically transformed contrast values. Each panel shows the analysis of one of the models, with simple cells indicated by open symbols and complex cells by filled symbols. The diagonal line on each graph is where mean error per data point is equal to variance per data point. For points above this line, error is greater than the variance. The points for the d-DOG-s model are distributed roughly evenly around the diagonal line (figure 11*a*); the remaining graphs (figure 11*b–e*) have been arranged in order of increasingly poor fits of the models to the data points. Data from simple cells and complex cells are similarly distributed throughout each plot. Hence, neither the variance of contrast sensitivity measurements, nor the error associated with the fit of any of the functions, would help to distinguish these two groups of cells. The order of quality of fit, from best to worst, indicated by figure 11 (*b–e*) is DOG-s, DOG, Gabor and D^2G. Thus, for the whole sample of cells studied, the DOG-based models (figure 11*a–c*) provide a better description of spatial-contrast sensitivity functions than the Gabor function (figure 11*d*) or the second differential of a Gaussian (figure 11*e*).

Although there are a few relatively large errors, greater than 0.02, for the sensitivity data fitted by the d-DOG-s model, these are almost invariably due to single individual data points that are far removed from the fitted curve. Whether these are truly characteristic of the particular spatial-contrast sensitivity function or whether they represent statistical outliers could be decided only by making repeated measurements on the same cell.

The distribution of error with respect to variance gives a good overall picture of the abilities of each model to describe the spatial-contrast sensitivity function, but it does not show whether there is an exclusive subset of cells for which a single model provides the optimal description, even though that model might be inappropriate for the majority of cells. To examine whether there was any clustering of neurons on the basis of the quality of fit, the errors associated with the application of two models were compared. Figure 12 shows the results of this comparison for each cell for the DOG-s, DOG, Gabor and D^2G (figure 12*a–d* respectively) plotted against the d-DOG-s model. It can be seen that the d-DOG-s model fits the contrast-sensitivity measurements of all cells at least as well as or better than any of the other models.

Further examples of spatial-contrast sensitivity functions that are well described by the d-DOG-s model are shown in the upper six panels of figure 13. These illustrate the wide variety of shapes found for cortical cells and the flexibility of the d-DOG-s model in accounting for them. The values of the parameters for the best-fitting version of the d-DOG-s model are shown in table 2. The lowest two panels show examples of cells for which the simple DOG model (figure 13*g*) or indeed a single Gaussian (figure 13*h*) are adequate to describe the data. The sensitivity function shown in figure 13*b* is one of the most narrowly tuned that we have encountered;

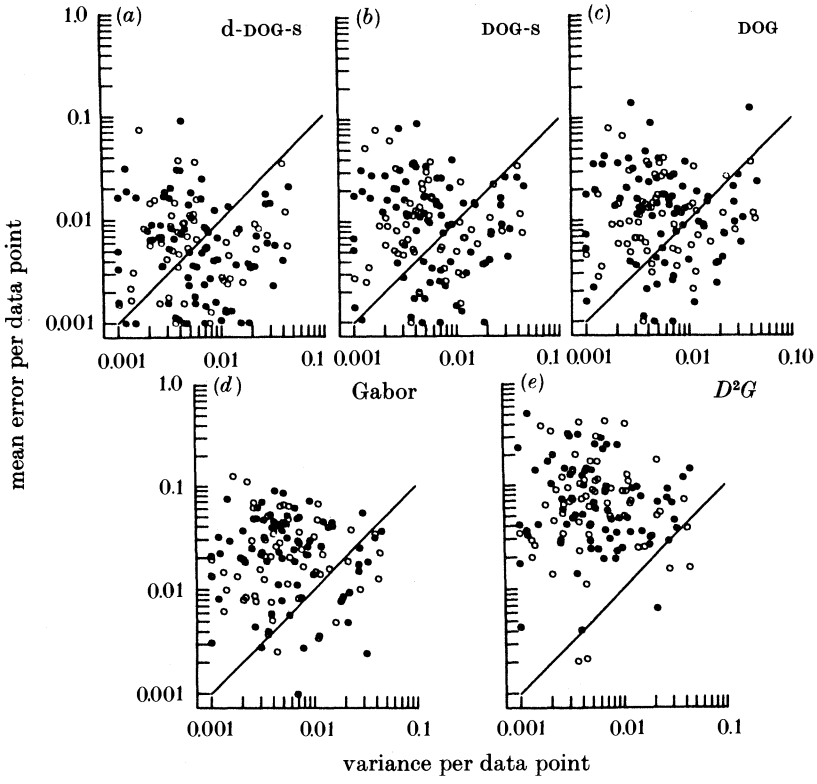

FIGURE 11. Relation between the mean error per data point and the mean variance per data point for each of the models fitted to every cell in our sample. The filled symbols represent measurements from 77 simple cells; the open symbols are from 61 complex cells. The solid line in each graph, with a slope of 1, indicates where the error is equal to the variance. A point below the diagonal line indicates that the error in fitting the model to the data is less than the variance associated with the sensitivity measurements for that cell. Conversely points above the line indicate that the error was greater than the variance; such points indicate cells that are relatively poorly fitted by the model. We have arranged the models from best to worst, based on the number of data points above the line of equality: (*a*), d-DOG-S; (*b*), DOG-S; (*c*), DOG; (*d*), Gabor; (*e*) D^2G.

as can be seen, its sensitivity function is well described by the d-DOG-S model and the associated spatial weighting function would have multiple antagonistic zones (Kulikowski & Bishop 1981; Kulikowski *et al.* 1982).

It is obviously to be expected that the d-DOG-S model will be as good as or better than the DOG-S and DOG functions, because elimination of some of the parameters from the d-DOG-S model produces the equations of DOG-S and DOG (i.e. DOG-S and DOG are straightforward reductions of d-DOG-S). Comparisons between d-DOG-S and the Gabor model (figure 12*c*) and d-DOG-S and the second differential of a Gaussian (figure 12*d*), indicate that there are no cells for which the Gabor or D^2G models provide a better description of the data than d-DOG-S. Of course, it should be remembered that the number of free parameters in the d-DOG-S model is greater

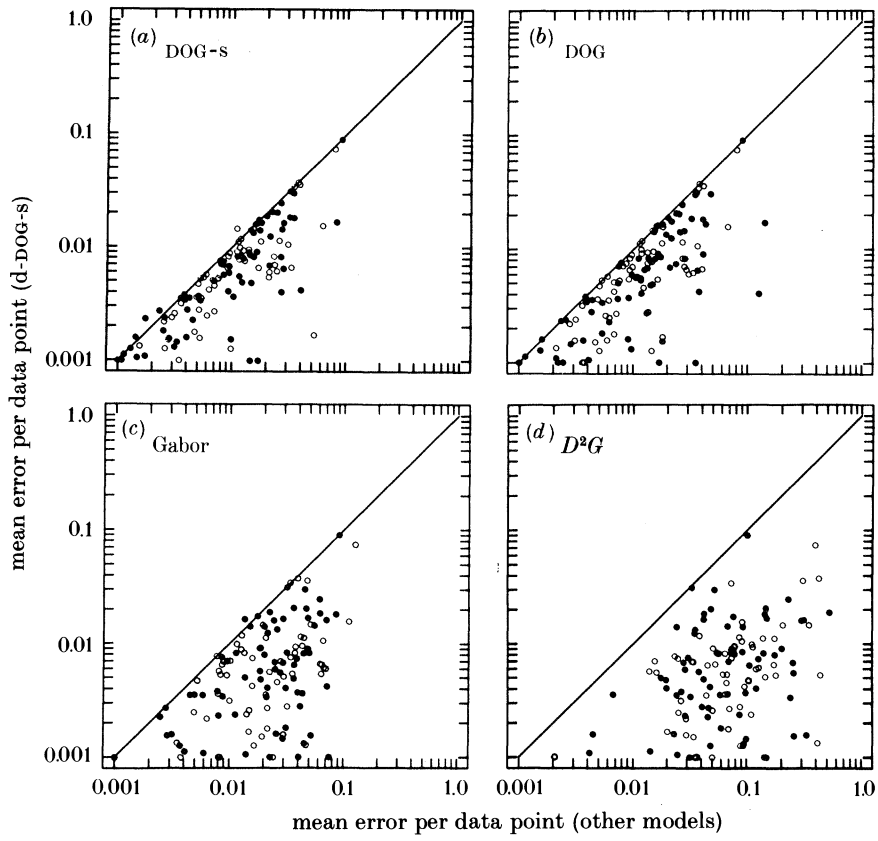

FIGURE 12. The mean error per data point for the best-fitting version of the d-DOG-S model (ordinate) is plotted against the mean error per data point for the other four models. Deviations below the solid line of equal error indicate a failure of the model represented on the abscissa to account for the spatial-contrast sensitivity function as well as the d-DOG-S model. The filled and unfilled symbols indicate simple and complex cells respectively, as in figure 11.

than both the Gabor and D^2G. However, both the DOG function and the Gabor function, as implemented, have four free parameters and therefore a simple comparison between them is justified.

In figure 14*d* we have explicitly compared these two models. The mean error associated with the best-fitting Gabor is plotted on the abscissa; the error for the DOG is shown on the ordinate. Cells whose sensitivity functions were equally well fitted by either the Gabor or the DOG would lie on the solid diagonal. Points below this line signify that the DOG produces a better fit than the Gabor, while those above the line favour the Gabor fit. Although the DOG model provides a better description of the majority of cells, there are some for which the Gabor function has a lower error than the simple DOG. For the neuron illustrated in figure 14, the Gabor function (figure 14*a*) fits the measured contrast-sensitivity values very well, having mean error of 0.0028. For comparison, the DOG fit (shown in figure 14*b*)

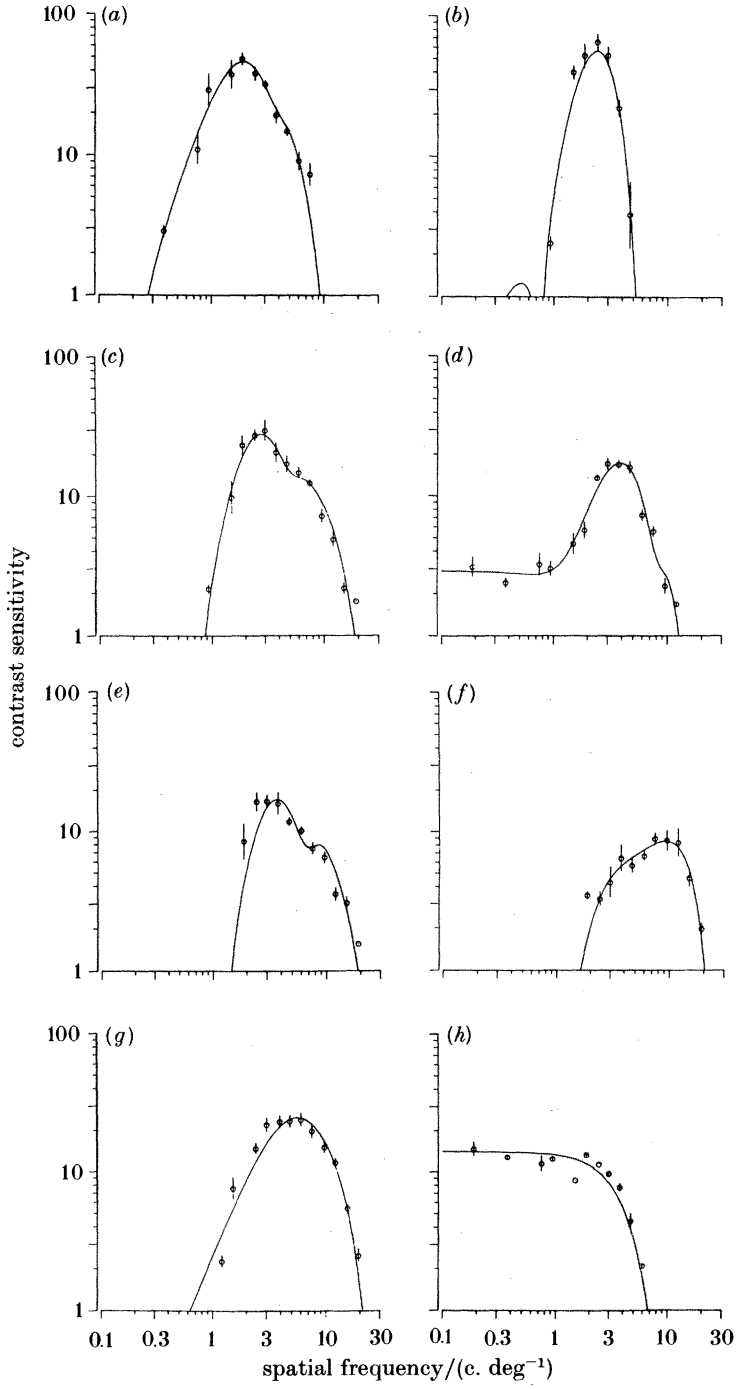

FIGURE 13. Panels (*a–f*) show the d-DOG-s model (equation A 1) fitted to the contrast-sensitivity functions of six neurons, to illustrate the variety of shapes of these functions and the ability of the model to describe them. The lowest two panels show examples of cells that were well fitted by the DOG model (*g*) and by a single Gaussian (*h*). Details of the parameters are given in table 2. The open circles indicate the mean value of contrast sensitivity and the error bars indicate ± one standard deviation from the mean. Cells in (*a*, *b*, *c*, *e*) had receptive fields between 1.0 and 1.5 degrees from the fovea; receptive fields of cells in *d*, *f*, *g* were within 0.5 degrees of the fovea; receptive field of cell in *h* was 3.0 degrees from the fovea.

TABLE 2. THE PARAMETER VALUES FOR THE BEST-FITTING VERSION OF d-DOG-s (*a–f*), DOG (*g*) AND A SINGLE GAUSSIAN (*h*) TO THE SPATIAL-CONTRAST SENSITIVITY FUNCTIONS SHOWN IN FIGURE 13

	sensitivity				space constant/arcmin				separation, S arcmin	symmetry, g	error	lamina	type (f_1/f_2)
	A_1	A_2	A_3	A_4	x_{c_1}	x_{s_1}	x_{c_2}	x_{s_2}					
a	48.7	14.8	39.1	4.4	4.07	5.99	8.40	33.6	12.5	0.5	0.0083	II/III	S(2.8)
b	97.8	97.7	97.8	97.7	7.59	13.1	7.29	14.3	8.88	0.5	0.0080	IVb	S(4.07)
c	20.0	20.0	20.0	20.0	1.79	12.1	5.45	15.4	9.88	0.5	0.0053	V	Cx(0.86)
d	20.5	15.2	9.5	7.1	2.73	5.56	3.02	11.7	7.38	0.5	0.0032	IVcα	S(1.63)
e	14.5	14.0	14.5	14.5	1.65	5.65	3.71	10.1	8.25	0.5	0.0135	II/III	Cx(0.92)
f	9.6	9.6	5.3	5.3	1.37	10.1	1.15	15.1	2.27	0.5	0.0054	IVcβ	Cx(0.73)
g	35.2	35.2	—	—	1.71	5.49	—	—	—	—	0.0063	VI	Cx(0.29)
h	14.1	—	—	—	4.62	—	—	—	—	—	0.0043	VI	S(4.03)

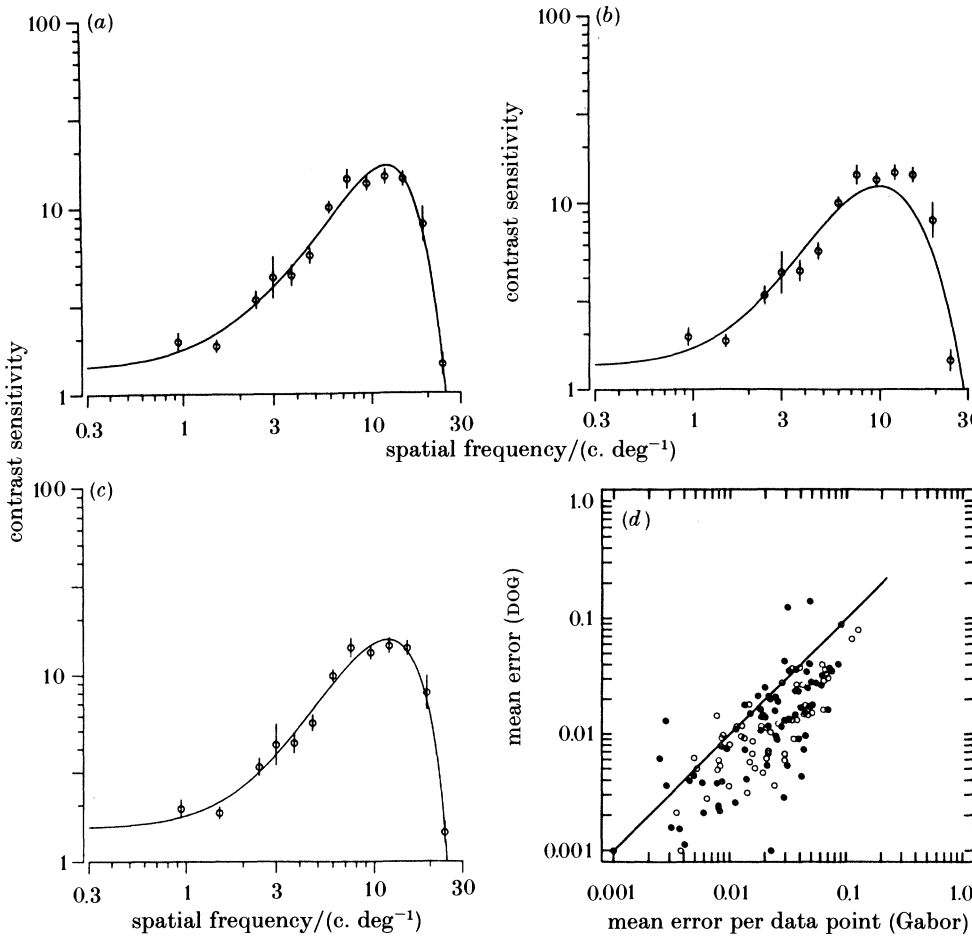

FIGURE 14. The upper two graphs show the contrast-sensitivity function from one of the few neurons for which the Gabor (*a*) shows a significantly better fit than the simple DOG (*b*). The mean error associated with the Gabor fit is 0.0028, and with the DOG, 0.0131. However, the DOG-S model (*c*) can fit the data with a similar error to the Gabor, 0.0023. The cell was classified as simple, with a receptive field 0.4° from the fovea, and was recorded in layer IVc. (*d*) Comparison of the mean error obtained from the best-fitting versions of the DOG and the Gabor functions for all cells. (Details as for figure 12.)

has a mean error of 0.0131, about five times greater than that of the Gabor. This is, in fact, the largest difference in favour of the Gabor of all the cells that we have tested. However, the DOG-S model (figure 14*c*) has a slightly *lower* error than the Gabor. Again, the addition of the separation parameter to the basic DOG model considerably improves the fit.

DISCUSSION

It is clear that, of the models considered in this paper, the d-DOG-S model can account most accurately for the spatial-contrast sensitivity functions of cortical neurons. Therefore, in spite of its many parameters, the d-DOG-S can be considered

as preferable for the determination of characteristics of tuning functions, such as bandwidth, peak spatial frequency, peak sensitivity and acuity, that are often quoted in comparison with those derived from psychophysical studies or in computational theories of early visual processing. For many cells, the reduced DOG-based models provide fits that are indistinguishable from the d-DOG-s model (figure 12*a*, *b*) and therefore provide simpler, yet adequate, descriptions of the spatial tuning. For a few cells, the Gabor function gives excellent fits to their spatial-contrast sensitivity functions (e.g. figure 14*a*), but over the whole sample of cells it is poorer than the DOG-based models (figures 12*c* and 14*d*). D^2G is just poor overall (figures 11*e* and 12*d*).

It is probably not surprising that the few explicit models of cortical receptive-field structure previously considered, based on the Gabor (Marcelja 1980), the DOG (Rose 1979) or on a restricted version of the d-DOG-s (Heggelund 1981; Soodak 1986) have all been deemed to be adequate, because they do, qualitatively, attain the general shape of a bandpass device. It is only when quantitative measures from a large sample of cortical neurons are examined comparatively that the differences between the various models become evident.

Receptive-field organization

Comparison of DOG-based models

Although the d-DOG-s and DOG-s models give better overall fits to the spatial contrast sensitivity functions than the simple DOG, their improved performance is at the expense of the introduction of extra free parameters, most significantly the separation parameter (S) that distinguishes the DOG-s and DOG models. However, it is possible to give an appealing functional interpretation of the separation parameter in terms of receptive-field organization. This is illustrated in figure 15, which shows the component Gaussians of the DOG (figure 15*a*) and the DOG-s (figure 15*c*), plotted with contrast sensitivity and spatial frequency on linear axes (dashed lines, centre mechanism; dotted lines, surround mechanism). The resultant combined functions, shown as solid lines in figure 15(*a*, *c*) are replotted in figure 15(*b*, *d*), but in the more familiar log–log coordinates. The DOG function, with spatially coincident peaks of the centre and surround mechanisms, obviously must have an individual Gaussian for the centre mechanism with a sensitivity that is greater than the peak of the resultant DOG. The sensitivity of the centre mechanism of the DOG is represented by the dashed line in figure 15*b*. In contrast, the DOG-s function, by virtue of the separation parameter, can attain the same peak sensitivity in the combined curve by using Gaussians whose peaks are *lower* than their combination.

The centre Gaussian of the DOG-s function (figure 15*d*, dashed line) has a peak amplitude of 29; the DOG-s function has a peak sensitivity of 43. This is because the effect of the surround Gaussian adds to that of the centre Gaussian at some spatial frequencies, owing to the difference in spatial phase introduced by the separation parameter (figure 15*c*, *d*). The two flanking regions forming the surround in the DOG-s model remain in even-symmetric, cosine phase just like the single Gaussian mechanism forming the surround in the DOG model. Thus the Fourier transform of the DOG-s function has real parts only, which are illustrated

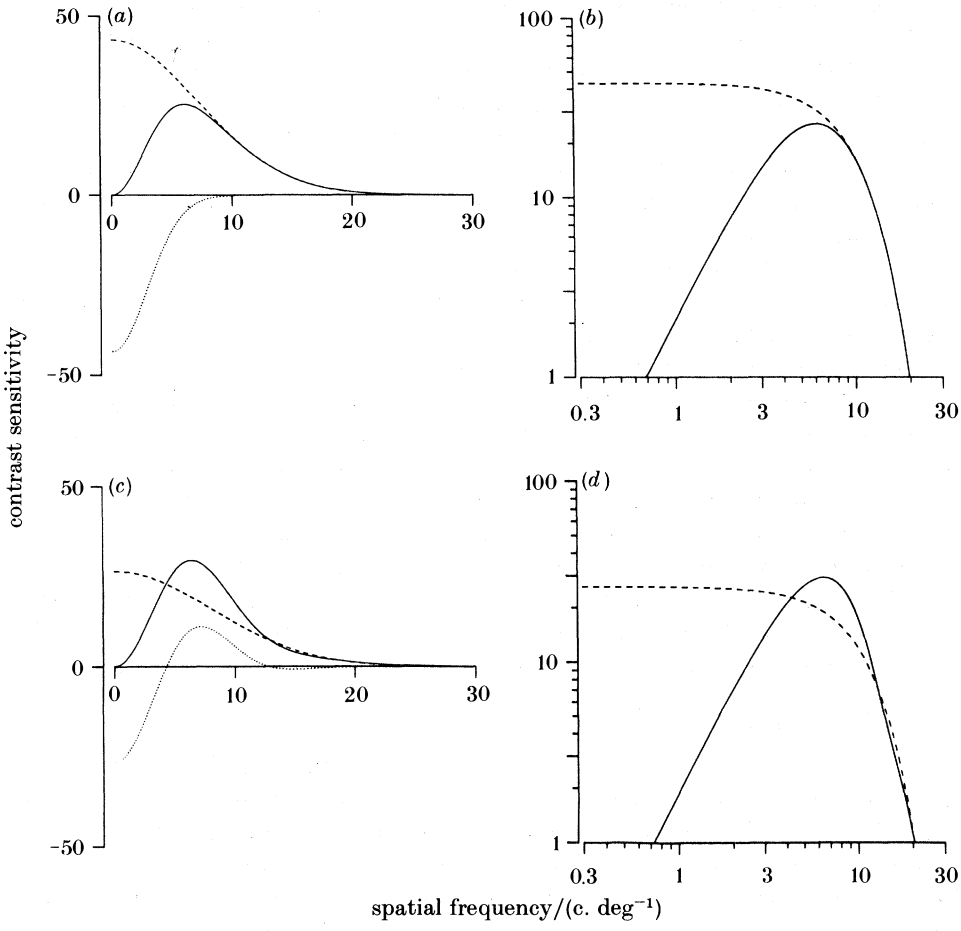

FIGURE 15. (*a*) The centre (dashed line) and surround (dotted line) Gaussians of a DOG function plotted on linear spatial-frequency and contrast-sensitivity axes. Because the peaks of the centre and surround Gaussians are spatially coincident, they subtract at all spatial frequencies. Therefore, to obtain a DOG of a given amplitude, the centre mechanism's sensitivity must be greater than the maximum sensitivity of the DOG. The combination of the centre and surround is shown by the solid line in (*a*). In (*b*) the solid line shows the same DOG as in (*a*), but on the more familiar log–log axes; the centre mechanism is shown by the dashed line. In (*c*) the centre (dashed line) and surround (dotted line) Gaussians of a DOG-S (solid line) function are shown on linear axes. The same DOG-S function as seen in (*c*) is shown in (*d*) on log–log axes. Note that the surround Gaussian is of the same sign as the centre Gaussian at some spatial frequencies (see Appendix). Thus the two Gaussians combine their sensitivities at these spatial frequencies with the result that the peak sensitivity attained by the DOG-S function, shown by the solid line in (*c*) and (*d*), is greater than the centre component alone (dashed line in (*c*) and (*d*)).

in figure 15(*c*, *d*). This fundamental effect of the separation factor would help the visual system, using the DOG-S configuration, to create spatial-contrast sensitivity functions with relatively narrow bandwidths, but without the attendant loss of sensitivity associated with narrow-band DOG functions (Marr & Hildreth 1980). These comments apply with even more force to the d-DOG-S model. Moreover, the

addition of the spatial separation between centre and surround mechanisms accounts for much of the improvement in the ability of the d-DOG-s and DOG-s models to fit the spatial-contrast sensitivity functions, when compared with the DOG function. This is especially so, when the sensitivities of the individual Gaussian mechanisms have been constrained, as in the implementation of all three DOG-based models described in this paper. As will be seen later in the Discussion, the upper limit on the amplitude of the individual Gaussians is reasonable when consideration is given to the properties of lateral geniculate cells that must, directly or indirectly, provide input to the cortical cells.

As shown in figure 1, for the hypothetical spatial-contrast sensitivity function, the inverse transform of the amplitude portion of the function can give spatial weighting profiles ranging from pure even-symmetric to odd-symmetric. Therefore it should be stressed that the best-fitting d-DOG-s functions do not uniquely specify the phase of the Fourier spectrum and therefore the relative strengths of the flanking regions. This point is exemplified in figure 16, which shows the versions of the d-DOG-s model that provide the best fit to the contrast-sensitivity data of the cell shown in figures 6–10*a*, where the phase parameter (g) has been constrained to give a pure even-symmetric (figure 16*a*), intermediate (figure 16*b*) or almost purely odd-symmetric (figure 16*c*) profile. It can be seen that, although the relative amplitude and spatial organization of the surround component in the spatial weighting functions changes, the resultant amplitude spectra are almost identical.

Subunits of cortical-cell receptive field

A major advantage of the DOG-based models is that they can be interpreted in terms of the organization of the components of the receptive field. As mentioned in the section describing the DOG-based models, in order to maintain the parameters of these models within reasonable bounds, quite strong constraints were imposed during the curve-fitting procedures. For example, the maximum sensitivity of the individual Gaussians was constrained to be no greater than 1.5 times the greatest sensitivity recorded for each cell. Although the exact value of this limit is somewhat arbitrary, the principle of setting a limit is very important. Otherwise, it would be possible for the DOG model to give a deceptively plausible description of a narrow-band spatial-contrast sensitivity function, such as that in figure 13*b*. If the fitting procedure were allowed to hypothesize very high sensitivities (greater than 250) for each Gaussian mechanism, the difference of the two would indeed be a high-sensitivity, relatively narrow-band function, but the existence of single Gaussian mechanisms of very high sensitivity as real single entities in the nervous system is physiologically implausible and certainly not experimentally verified (Kaplan & Shapley 1982; Derrington & Lennie 1984).

In general, with the well-fitting DOG-s and d-DOG-s models, the parameters selected by the fitting procedure were well away from the bounds imposed by the constraints. In fact, the parameters selected by these models are highly compatible with the properties of lateral geniculate inputs (Kaplan & Shapley 1982; Derrington & Lennie 1984). For example, the centre-mechanism space constants are in the range 0.5–8.0′, for cells with receptive-field centres within one degree of the fovea, and this range shifts systematically with eccentricity. Even for the small range of eccentricities studied in this work, the shift is evident and is similar to that seen

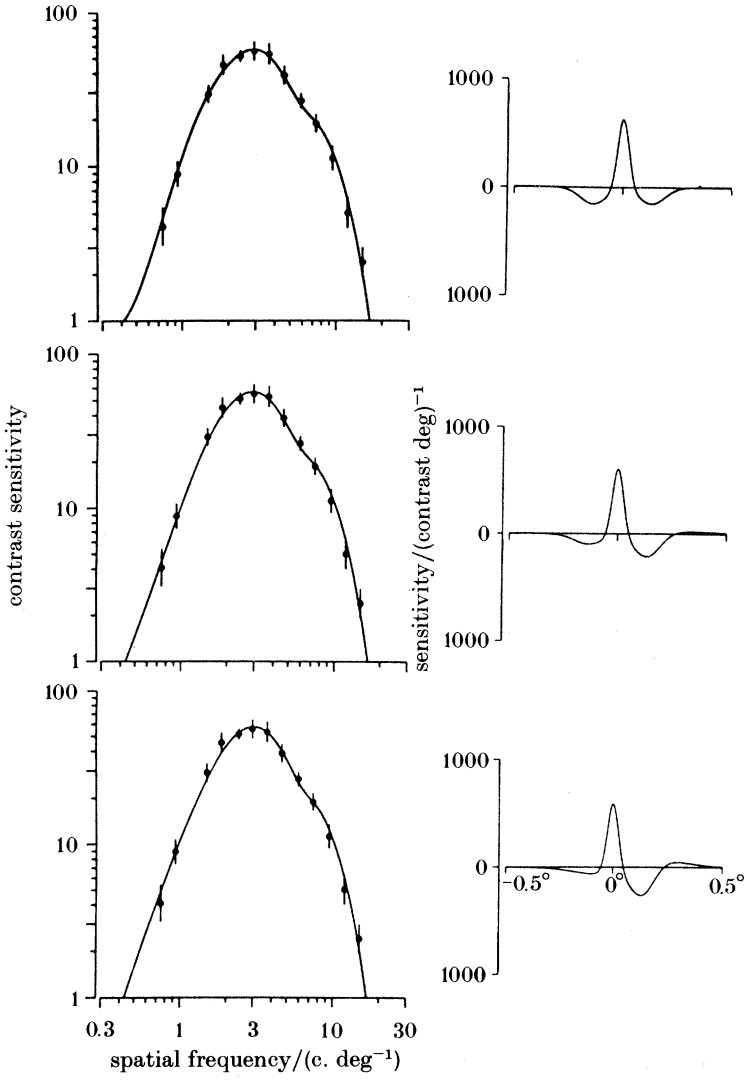

FIGURE 16. The graphs show the version of the d-DOG-s model that fit best to the contrast sensitivity data of the cell in figure 6*a*, where the model varies from: (*a*) pure even symmetry, the symmetry parameter, $g = 0.5$; (*b*) through intermediate symmetry, $g = 0.26$; (*c*) to almost pure odd symmetry, $g = 0.0$ (See legend to figure 3.) All the other parameters were free to vary. The figure shows that, within the constraints of the d-DOG-s model, the relative amplitudes and spatial organization of the flanking subregions may change without any marked change in the amplitude spectrum. It is worth noting that the separation parameter stays almost constant, at around 8′, in all three fits, despite the change of symmetry of the flanking regions.

for geniculate cells. Although these measures are derived from the application of a model, it should be stressed that they would be difficult to extract by other means. For example, the models separate out the differences in the sensitivities of the individual mechanisms from the differences in their spatial sizes. Further, use of the model gives some insight into how mechanisms could be combined to

produce the overall receptive-field profile. For example, figure 15 illustrates how inputs derived from parvocellular LGN cells, even though they generally have peak sensitivities lower than 25, could be used to build cortical-cell receptive fields with a sensitivity higher than 25 at some spatial frequencies. Another mechanism for enhancing sensitivity in the cortex could be summation along the axis of preferred orientation. Finally, it is encouraging that some of the parameters of the receptive field are robustly defined, even when results from different models are compared (see figures 6–8).

One of the remarkable features of our data is that no distinction can be drawn between simple and complex cells on the basis of the models describing their spatial-contrast sensitivity functions. However, in terms of line-weighting functions, there is a marked difference between the two cell classes in the cat cortex (Movshon *et al.* 1978*a*, *b*). There are several lines of evidence that suggest that complex cell receptive fields are made up of the nonlinear combination of subunits, which themselves show linear spatial summation (Movshon *et al.* 1978*b*; Spitzer & Hochstein 1985*a*, *b*). If these linearly summating subunits have characteristics rather like those of simple cells in nearby areas of cortex, then it would be expected that no major differences between simple and complex cells would be found, in terms of their spatial-contrast sensitivity functions. The similarity of simple cells and the linearly summating subunits of complex cells argues that they may have common sources of input from the LGN.

Anatomical considerations

A consequence of a relatively simple, yet accurate, model of the spatial weighting of striate neurons is that it allows some of the parameters to be tested against the anatomical distribution of inputs to cells. An intriguing feature suggested by the d-DOG-s and DOG-s models is that the peaks of some of the surrounds (or flanking regions) of receptive fields are separated from the centre mechanism by about 10′ for cells with receptive fields within a degree of the foveal representation. A value of 10′ with a magnification factor of 15 mm deg^{-1}, which is perhaps a conservative estimate (Dow *et al.* 1981), indicates possible interactions, based on strict topographic order, over distances of 2–3 mm across the cortex. Thus there could well be a correlation between the orderly distribution of patch-like lattices seen in the anatomical arrangement of intracortical connections (Rockland *et al.* 1982) and the structure of the receptive fields. This would eliminate the need for any ill-defined concepts, such as long-range inhibitory influences or global 'pools' of non-specific inhibition in which cortical cells supposedly sit. Rather, the long-range connections can be seen as providing the anatomical basis for the straightforward, classically defined and well-documented features of receptive-field organization.

Implications for visual processing

Cortical neurons display a wide variety of selectivities other than those defined in the models studied here. Thus the overall picture of cortical-cell receptive fields provided by the models is incomplete, in that selectivity for direction and speed of motion, orientation, chromaticity or disparity is currently not included in the

models. Despite the restricted nature of the models, some general conclusions about visual mechanisms can be made.

One consequence of using a poorly fitting model to process our results would be that the extraction of parameters of the function, such as bandwidth and peak frequency, would, in many cases, represent the data inaccurately. This might have serious consequences for the performance of a theoretical model of subsequent visual function that used the Gabor or D^2G for preliminary filtering. Furthermore, because a number of theoretical models of early visual processing underpin their use of the Gabor function by appealing to its property of minimizing conjoint uncertainty in space and spatial frequency, the failure of the Gabor function to match actual data from cortical cells suggests that this property is of limited significance for visual processing in the primate striate cortex. Whether the receptive fields of neurons in the extra-striate visual areas adhere to the Gabor shape or whether the characteristics of some cells in the striate cortex are close enough in shape to the Gabor function for its optimizing property to be adequately retained are matters for further experimental investigation. Rather similar points apply to D^2G and modifications of it (Marr & Hildreth 1980; Marr & Ullman 1981).

Our preferred models for cortical-cell receptive-field profiles are obviously not in accord with any previously proposed principles of computational vision (unlike, say, the use of ∇^2G functions to find zero crossings). The first stage in the application of such principles to a biological visual system must be an accurate model of the elements of the system. It is therefore worth considering what are the most marked differences between the shapes of filters, such as d-DOG-s, Gabor and D^2G. In the spatial frequency domain, two features are apparent. First, cortical cells tend to have spatial-contrast sensitivity functions that are roughly symmetric when plotted on a logarithmic frequency axis rather than a linear one. Gabor and D^2G functions are closer to symmetry on a linear frequency axis. A related feature is that the low-frequency cut of cortical cells is much steeper than either Gabor or D^2G would predict. None the less, the bandwidths of cortical cells are not very narrow (DeValois *et al.* 1982). So appealing to a more narrowly tuned function, such as a higher-order differential, would not produce a significant improvement.

In the space domain, these features imply that the spatial extent of the receptive field, particularly its 'inhibitory' flanking region, is greater than would be predicted from a Gabor or D^2G function. Before Marr & Hildreth's work on edge detection, the majority of edge detectors in computer vision systems worked on quite small regions of support (typically 3–6 pixels in linear extent). Marr & Hildreth (1980) introduced filters with considerably larger regions of support (approximately 30 pixels in linear extent). Adopting the d-DOG-s model suggests that the size should be bigger still for efficient edge detection and localization. Moreover, even when receptive fields have quite small centre mechanisms, they may have quite large 'inhibitory' flanking regions.

The suitability of cortical receptive fields for edge detection and localization is emphasized by observations we have presented elsewhere. Localization thresholds for simple cells are in the hyperacuity range, both when measured directly and when derived from calculations based on the DOG model of the receptive field

(Parker & Hawken 1985), indicating that the performance of individual neurons is well within the range found for human psychophysical observers. This is a case where the experimental determination of a spatial-contrast sensitivity function, followed by the application of a straightforward model of the receptive field, results in testable predictions of the cell's behaviour.

Finally, it is obvious that the DOG-based models discussed here are similar, in many ways, to the original models of simple cells proposed by Hubel & Wiesel (1962). It has been suggested (DeValois *et al.* 1985) that the investigation of cortical cells with grating stimuli has revealed additional forms of receptive-field organization that invalidate the Hubel & Wiesel model. It is ironic that the quantitative analysis presented here favours simple modifications of Hubel & Wiesel's model rather than schemes, such as the Gabor filters, that have been specifically inspired by the frequency-domain approach to visual processing.

This work was supported by MRC grants G979/49 and 7900491 to Colin Blakemore and USAF Grant AFOSR-85-0296. A.J.P. was supported by a Light Research Fellowship at St Catherine's College, Oxford. We thank Dr I. Vlachonikolis (Department of Biomathematics, Oxford) for advice on statistics. We are particularly grateful to Colin Blakemore, David Tolhurst and Tony Movshon for helpful comments.

REFERENCES

Andrews, B. W. & Pollen, D. A. 1979 Relationship between spatial frequency selectivity and receptive field profile of simple cells. *J. Physiol., Lond.* **287**, 163–176.

Bishop, P. O., Henry, G. H. & Smith, C. J. 1971 Binocular interaction fields of single units in the cat striate cortex. *J. Physiol., Lond.* **216**, 39–68.

Blakemore, C. & Campbell, F. W. 1969 On the existence of neurones in the human visual system selectively sensitive to the orientation and size of retinal images. *J. Physiol., Lond.* **203**, 237–260.

Blakemore, C. & Vital-Durand, F. 1981 Distribution of X- and Y-cells in the monkey's lateral geniculate nucleus. *J. Physiol., Lond.* **320**, 17*P*–18*P*.

Braddick, O. J., Campbell, F. W. & Atkinson, J. 1978 Channels in vision: basic aspects. In *Handbook of sensory physiology, vol.* 8 (*Perception*) (ed. R. Held, H. W. Leibowitz & H.-L. Teuber), pp. 1–38. Heidelberg: Springer.

Campbell, F. W. & Robson, J. G. 1968 Application of Fourier analysis to the visibility of gratings. *J. Physiol., Lond.* **197**, 551–566.

Cooper, G. F. & Robson, J. G. 1968 Successive transformations of visual information in the visual system. *I.E.E. N.P.L. Conf. Proc.* **42**, 134–143. London: I.E.E.

Daugman, J. D. 1984 Spatial visual channels in the Fourier plane. *Vision Res.* **24**, 891–910.

Daugman, J. D. 1985 Uncertainty relation for resolution in space, spatial frequency, and orientation optimized by two-dimensional visual cortical filters. *J. opt. Soc. Am.* A **2**, 1160–1169.

Dawis S., Shapley, R. M., Kaplan, E. & Tranchina, D. 1984 The receptive field organization of X-cells in the cat: spatiotemporal coupling and asymmetry. *Vision Res.* **24**, 549–564.

Dean, A. F. & Tolhurst, D. J. 1983 On the distinctness of simple and complex cells in the visual cortex of the cat. *J. Physiol., Lond.* **344**, 305–325.

Derrington, A. M. & Lennie, P. 1982 The influence of temporal frequency and adaptation level on receptive field organization of retinal ganglion cells in the cat. *J. Physiol., Lond.* **333**, 343–366.

Derrington, A. M. & Lennie, P. 1984 Spatial and temporal contrast sensitivities of neurones in the lateral geniculate nucleus of the macaque. *J. Physiol., Lond.* **357**, 219–240.

DeValois, R. L., Albrecht, B. G. & Thorell, L. G. 1982 Spatial frequency selectivity of cells in macaque visual cortex. *Vision Res.* **22**, 545–599.

DeValois, R. L., Thorell, L. G. & Albrecht, D. G. 1985 Periodicity of striate-cortex-cell receptive fields. *J. opt. Soc. Am.* A **2**, 1115–1123.

Dow, B. M., Snyder, A. Z., Vautin, R. G. & Bauer, R. 1981 Magnification factor and receptive field size in the foveal striate cortex of the monkey. *Expl Brain Res.* **44**, 213–228.

Draper, N. & Smith, H. 1966 *Applied regression analysis.* New York: J. Wiley & Sons, Inc.

Eldridge, J. L. 1979 Reversible ophthalmoscope using a corner-cube. *J. Physiol., Lond.* **295**, 1–2*P*.

Enroth-Cugell, C. & Robson, J. G. 1966 The contrast sensitivity of retinal ganglion cells of the cat. *J. Physiol., Lond.* **187**, 517–552.

Enroth-Cugell, C., Robson, J. G., Schweitzer-Tong, D. E. & Watson, A. B. 1983 Spatio-temporal interactions in cat retinal ganglion cells showing linear spatial summation. *J. Physiol., Lond.* **341**, 279–307.

Field, D. J. & Tolhurst, D. J. 1986 The structure and symmetry of simple-cell receptive-field profiles in the cat's visual cortex. *Proc. R. Soc. Lond.* B **228**, 379–400.

Gilbert, C. G. 1977 Laminar differences in receptive field properties of cells in cat primary visual cortex. *J. Physiol., Lond.* **268**, 391–421.

Hawken, M. J. & Parker, A. J. 1984 Contrast sensitivity and orientation selectivity in lamina IV of the striate cortex of Old World monkeys. *Expl Brain Res.* **54**, 367–372.

Heggelund, P. 1981 Receptive field organization of simple cells in cat striate cortex. *Expl Brain Res.* **42**, 89–98.

Hochstein, S. & Shapley, R. M. 1976 Quantitative analysis of retinal ganglion cell classifications. *J. Physiol., Lond.* **262**, 237–264.

Hubel, D. H. & Wiesel, T. N. 1961 Integrative action in the cat's lateral geniculate body. *J. Physiol., Lond.* **155**, 385–398.

Hubel, D. H. & Wiesel, T. N. 1962 Receptive fields, binocular interaction and functional architecture in cat's visual cortex. *J. Physiol., Lond.* **160**, 106–154.

Hubel, D. H. & Wiesel, T. N. 1965 Receptive fields and functional architecture in two non-striate visual areas (18 and 19) of the cat. *J. Neurophysiol.* **28**, 229–289.

Hubel, D. H. & Wiesel, T. N. 1968 Receptive fields and functional architecture of monkey striate cortex. *J. Physiol., Lond.* **195**, 215–243.

Kaplan, E. & Shapley, R. M. 1982 X and Y cells in the lateral geniculate nucleus of macaque monkeys. *J. Physiol., Lond.* **330**, 125–143.

Kulikowski, J. J. & Bishop, P. O. 1981 Linear analysis of the responses of simple cells in the cat visual cortex. *Expl Brain Res.* **44**, 386–400.

Kulikowski, J. J., Marcelja, S. & Bishop, P. O. 1982 Theory of spatial position and spatial frequency relations in the receptive fields of simple cells in the visual cortex. *Biol. Cybernet.* **43**, 187–198.

Levick, W. R. & Thibos, T. N. 1980 Orientation bias of cat retinal ganglion cells. *Nature, Lond.* **286**, 389–390.

Linsenmeier, R. A., Frishman, L. J., Jakiela, H. G. & Enroth-Cugell, C. 1982 Receptive field properties of X and Y cells in the cat retina derived from contrast sensitivity measurements. *Vision Res.* **22**, 1173–1183.

Marčelja, S. 1980 Mathematical description of the responses of simple cortical cells. *J. opt. Soc. Am.* **70**, 1297–1300.

Marr, D. 1982 *Vision.* San Francisco: W. H. Freeman & Co.

Marr, D. & Hildreth, E. 1980 Theory of edge detection. *Proc. R. Soc. Lond.* B **207**, 187–217.

Marr, D. & Ullman, S. 1981 Directional selectivity and its use in early visual processing. *Proc. R. Soc. Lond.* B **211**, 151–180.

Merrill, E. G. & Ainsworth, A. 1972 Glass-coated platinum-plated tungsten microelectrodes. *Med. biol. Engng.* **10**, 662–672.

Movshon, J. A., Thompson, I. D. & Tolhurst, D. J. 1978*a* Spatial summation in the receptive field of simple cells in the cat's striate cortex. *J. Physiol., Lond.* **283**, 53–77.

Movshon, J. A., Thompson, I. D. & Tolhurst, D. J. 1978*b* Receptive field organization of complex cells in the cat's striate cortex. *J. Physiol., Lond.* **283**, 79–99.

Parker, A. J. & Hawken, M. J. 1985 The capabilities of monkey cortical cells in spatial resolution tasks. *J. opt. Soc. Am.* A **2**, 1101–1114.

Parker, A. J. & Hawken, M. J. 1987 Threshold detection of luminance contrast by neurons in the primate striate cortex: a comparison with psychophysical performance (In preparation.)
Robson, J. G. 1975 Receptive fields: spatial and intensive representations of the visual image. In *Handbook of perception*, vol. 5 (ed. D. Carterette & W. Friedman), pp. 81–115. New York: Academic Press.
Robson, J. G. 1983 Frequency domain visual processing. In *Physical and biological processing of images* (ed. O. J. Braddick & A. C. Sleigh), pp. 73–87. Berlin: Springer-Verlag.
Rockland, K. S., Lund, J. S. & Humphrey, A. L. 1982 Anatomical banding of intrinsic connections in the striate cortex of tree shrews (*Tupaia glis*). *J. comp. Neurol.* **209**, 41–58.
Rodieck, R. W. 1965 Quantitative analysis of cat retinal ganglion cell response to visual stimuli. *Vision Res.* **5**, 583–601.
Rose, D. 1979 Mechanisms underlying the receptive field properties of neurons in cat visual cortex. *Vision Res.* **19**, 533–544.
Sakitt, B. & Barlow, H. B. 1982 A model for the economical encoding of the visual image in cerebral cortex. *Biol. Cybernet.* **43**, 97–108.
Shapley, R. M., Kaplan, E. & Soodak, R. E. 1981 Spatial summation and contrast sensitivity of X and Y cells in the lateral geniculate nucleus of the macaque. Nature, *Lond.* **292**, 543–545.
Soodak, R. E. 1986 The spatial organization of visual receptive fields in the geniculostriate system of the cat. Ph.D. thesis, Rockefeller University.
Spitzer, H. & Hochstein, S. 1985*a* Simple- and complex-cell response dependences on stimulation parameters. *J. Neurophysiol.* **53**, 1244–1265.
Spitzer, H. & Hochstein, S. 1985*b* A complex-cell receptive field model. *J. Neurophysiol.* **53**, 1266–1286.
Watson, A. B. 1983 Detection and recognition of simple spatial forms. In *Physical and biological processing of images.* (ed. O. J. Braddick & A. C. Sleigh), pp. 100–114. Berlin: Springer-Verlag.
Watt, R. J. & Morgan, M. J. 1985 A theory of the primitive code in human vision. *Vision Res.* **25**, 1661–1674.
Wetherill, G. B. & Levitt, H. 1965 Sequential estimation of points on a psychometric function. *Br. J. math. statist. Psychol.* **18**, 1–10.
Wiesel, T. N. & Hubel, D. H. 1966 Spatial and chromatic interactions in the lateral geniculate body of the rhesus monkey. *J. Neurophysiol.* **29**, 1115–1156.
Wilson, H. R. & Bergen, J. R. 1979 A four mechanism model for threshold spatial vision. *Vision Res.* **19**, 19–32.
Yuille, A. & Poggio, T. 1985 Fingerprints theorems for zero-crossings. *J. opt. Soc. Am.* A**2**, 683–692.

Appendix

This Appendix documents the equations used to describe the models and gives some guidance on the interpretation of the parameters associated with the models. The Fourier transform of these models is, in general, complex and the amplitude portion of the Fourier transform was used to fit the measured spatial-contrast sensitivity function. However, because the line-weighting function indicates the structure of the models much more clearly, the equation specifying each model is the line-weighting function.

Models based on difference-of-Gaussian functions

These models consist of the algebraic sum of a number of Gaussian terms, each of which is specified by a scaling factor (k_c, k_s, etc.) and a space constant (x_c, x_s, etc).

Units

The terms x, x_c, x_s, S, etc. are measured in degrees of visual angle; f is measured in cycles per degree; k_c, k_s, etc. are measured in units of sensitivity per degree (see figures 6–10, right-hand graphs).

The terms $k_c \sqrt{\pi}\, x_c$, etc., which appear in the Fourier transform, can be usefully considered as a single constant with units corresponding to the conventional measure of contrast sensitivity for grating stimuli. For convenience, in the figure legends 6–10 the sensitivity constants are expressed as a single value (e.g. A, B) in this way. The equivalences between these two notations are indicated with the equations stating the line-weighting function for each model.

Difference of difference of Gaussians with separation (d-DOG-S)

$$\begin{aligned} &k_{c_1} \exp[-(x/x_{c_1})^2] - k_{s_1} \exp[-(x/x_{s_1})^2] \\ &-g[\![k_{c_2} \exp\{-[(x+S)/x_{c_2}]^2\} - k_{s_2} \exp\{-[(x+S)/x_{s_2}]^2\}]\!] \\ &(1-g)[\![k_{c_2} \exp\{-[(x-S)/x_{c_2}]^2\} - k_{s_2} \exp\{-[x-S)/x_{s_2}]^2\}]\!], \end{aligned} \tag{A 1}$$

where the constraint

$$(k_{c_1} - k_{s_1}) - (k_{c_2} - k_{s_2}) = 0$$

is applied and the equivalences to figure 6 are

$$A_1 = k_{c_1} \sqrt{\pi}\, x_{c_1}; \quad A_2 = k_{s_1} \sqrt{\pi}\, x_{s_1}; \quad A_3 = k_{c_2} \sqrt{\pi}\, x_{c_2}; \quad A_4 = k_{s_2} \sqrt{\pi}\, x_{s_2}.$$

Difference of Gaussians with separation (DOG-S)

$$k_c \exp[-(x/x_c)^2] - 0.5\, k_s \exp\{-[(x+S)/x_s]^2\} - 0.5\, k_s \exp\{-[(x-S)/x_s]^2\}, \tag{A 2}$$

where the equivalences to figure 7 are

$$B_1 = k_c \sqrt{\pi}\, x_c; \quad B_2 = k_s \sqrt{\pi}\, x_s.$$

Difference of Gaussians (DOG)

$$k_c \exp[-(x/x_c)^2] - k_s \exp[-(x/x_s)^2], \tag{A 3}$$

where the equivalences to figure 8 are

$$C_1 = k_c \sqrt{\pi}\, x_c; \quad C_2 = k_s \sqrt{\pi}\, x_s.$$

Fourier transforms

The Fourier transform of the sum of a number of functions is simply the sum of the Fourier transforms of those functions. The difference-of-Gaussian models can therefore be treated by examining the contribution of individual terms to the overall transform.

Terms of the form

$$k_c \exp[-(x/x_c)^2]$$

have Fourier transforms of the form:

$$k_c \sqrt{\pi}\, x_c \exp(-\pi^2 f^2 x_c^2).$$

Terms of the form

$$0.5\,k_s \exp\{-[(x+S)/x_s]^2\}+0.5\,k_s \exp\{-[(x-S)/x_s]^2\}$$

have Fourier transforms of the form:

$$k_s \sqrt{\pi}\, x_s \exp(-\pi^2 f^2 x_s^2) \cos(2\pi f S)$$

An example of this behaviour is shown in figure 15.
Terms of the form

$$0.5\,k_s \exp\{-[(x+S)/x_s]^2\}-0.5\,k_s \exp\{-[(x-S)/x_s]^2\}$$

have Fourier transforms of the form:

$$k_s \sqrt{\pi}\, x_s \exp(-\pi^2 f^2 x_s^2) \sin(2\pi f S).$$

Gabor function

$$k_c \exp[-(x/x_c)^2] \cos(2\pi f_c x+p). \tag{A 4}$$

The Fourier transform of a Gabor function (a sinusoid multiplied by a Gaussian envelope) is a pair of Gaussian spectra centred at the frequency (f_c) of the sinusoid, one at $+f_c$, the other at $-f_c$. The relative signs of these spectra depend on the phase (p) of the sinusoid. If both are positive or both are negative, then the sinusoid is in cosine phase relative to the peak of the spatial Gaussian envelope. If one is positive and the other is negative, then the sinusoid is in sine phase. Note that this latter arrangement guarantees that a receptive field with this characteristic will have zero sensitivity at zero spatial frequency. The constant D_1 in figure 9 simply scales the height of the Gaussian spectra in the frequency domain, but it does not have a simple structural interpretation as do the constants for the DOG-based models.

Second differential of a Gaussian

$$(2k_c/x_c^2)(1-2x^2/x_c^2) \exp[-(x/x_c)^2]. \tag{A 5}$$

The Fourier transform of this function can be understood most easily by noting that a differentiation in the space domain is equivalent to multiplying the frequency spectrum by the complex quantity $2\pi jf$. The Fourier transform of the second differential of a Gaussian is therefore dominated by a quadratic term at low spatial frequencies and a Gaussian term at high spatial frequencies. The constant E_1 in figure 10 is simply a scaling factor.